Carderock Division, Naval Surface Warfare Center

Bethesda, Maryland 20084-5000

NSWCCD-SIG-96/014-7250 February 1996

Signatures Directorate

Technical Report

The Calculation and Measurement of Flexural and Longitudinal Structural Power Flow on a Tee-Shaped Beam

by

Richard P. Szwerc

Stephen A. Hambric

MAJOR CARDEROCK DIVISION TECHNICAL COMPONENTS

CODE 011 Director of Technology

10 Machinery Systems/Programs and Logistics Directorate

20 Ship Systems and Programs Directorate

50 Hydromechanics Directorate

60 Survivability, Structures and Materials Directorate

70 Signatures Directorate

80 Machinery Research and Development Directorate

90 Machinery In-Service Engineering Directorate

CARDEROCK DIVISION, NSWC, ISSUES THREE TYPES OF REPORTS:

1. **CARDEROCKDIV reports, a formal series,** contain information of permanent technical value. They carry a consecutive numerical identification regardless of their classification or the originating directorate.

2. **Directorate reports, a semiformal series,** contain information of a preliminary, temporary, or proprietary nature or of limited interest or significance. They carry an alphanumerical identification issued by the originating directorate.

3. **Technical memoranda, an informal series,** contain technical documentation of limited use and interest. They are primarily working papers intended for internal use. They carry an identifying number which indicates their type and the numerical code of the originating directorate. Any distribution outside CARDEROCKDIV must be approved by the head of the originating directorate on a case-by-case basis.

REPORT DOCUMENTATION PAGE

1a. REPORT SECURITY CLASSIFICATION: UNCLASSIFIED	1b. RESTRICTIVE MARKINGS
2a. SECURITY CLASSIFICATION AUTHORITY	3. DISTRIBUTION / AVAILABILITY OF REPORT: Approved for Public Release; Distribution is unlimited
2b. DECLASSIFICATION / DOWNGRADING SCHEDULE	
4 PERFORMING ORGANIZATION REPORT NUMBER(S): NSWCCD-SIG-96/014-7250	5. MONITORING ORGANIZATION REPORT NUMBER(S)
6a. NAME OF PERFORMING ORGANIZATION: Naval Surface Warfare Ctr; 6b OFFICE SYMBOL (If applicable): 7250	7a. NAME OF MONITORING ORGANIZATION
6c ADDRESS (City, State, and ZIP Code): Code 7250, Bethesda, Md 20084-5000	7b. ADDRESS (City, State, and ZIP Code)
8a. NAME OF FUNDING / SPONSORING ORGANIZATION: Office of Naval Research; 8b. OFFICE SYMBOL (If applicable): 0233	9. PROCUREMENT INSTRUMENT IDENTIFICATION NUMBER
8c ADDRESS (City, State, and ZIP Code): Ballston Towers, Arlingtonm Virginia	10. SOURCE OF FUNDING NUMBERS: PROGRAM ELEMENT NO. 0602323N; PROJECT NO.; TASK NO.; WORK UNIT ACCESSION NO.

11 TITLE (Include Security Classification): The Calculation and Measurement of Flexural and Longitudinal Structural Power Flow on a Tee Shaped Beam

12 PERSONAL AUTHOR(S): Szwerc, R. P. and Hambric, S.A.

13a TYPE OF REPORT	13b. TIME COVERED	14. DATE OF REPORT (Year, Month, Day)	15. PAGE COUNT
Technical	FROM 11/94 TO 12/95	February 1996	56

16 SUPPLEMENTARY NOTATION

17 COSATI CODES			18. SUBJECT TERMS (Continue on reverse if necessary and identify by block number)
FIELD	GROUP	SUB-GROUP	Power FLow, Structual Intensity, Flexural, Longitudinal

19 ABSTRACT (Continue on reverse if necessary and identify by block number)

A method for the simultaneous measurement of both longitudinal and flexural wave intensities in beams is developed and measurements are then conducted on three specimens: a straight beam, a continuous T-beam, and a bolted T-beam. The work demonstrates that discontinuities in structures help to interchange large amounts of power between the two wave types. The straight beam serves to validate the measurement techniques. Successful comparisons are made to predicted power levels on a finite element model of the T-beam . The bolted T-beam shows the power flow is reduced across the bolted joint when compared to the continuous T-beam. The validated experimental results will form the basis for the validation of techniques (to be developed) to measure as well as calculate structural intensity in the presence of longitudinal and flexural waves.

20 DISTRIBUTION / AVAILABILITY OF ABSTRACT: ☒ UNCLASSIFIED/UNLIMITED ☐ SAME AS RPT. ☐ DTIC USERS	21. ABSTRACT SECURITY CLASSIFICATION: UNCLASSIFIED
22a NAME OF RESPONSIBLE INDIVIDUAL: Richard P. Szwerc	22b. TELEPHONE (Include Area Code): 301-227-1252; 22c. OFFICE SYMBOL: 7250

DD FORM 1473, 84 MAR — 83 APR edition may be used until exhausted. All other editions are obsolete.

THIS PAGE INTENTIONALLY LEFT BLANK

List of Figures

Symbols

a_1 - resultant acceleration at position 1

a_{1T} - acceleration at position 1 on top of beam

a_{1B} - acceleration at position 1 on bottom of beam

a_2 - resultant acceleration at position 2

a_{2T} - acceleration at position 2 on top of beam

a_{2B} - acceleration at position 2 on bottom of beam

b - beam width

f - frequency, Hz

h - beam height

k - wave number

k_B - flexural wave (bending) wave number

m - mass per unit width

m' - mass per unit length

q - as subscript, refers to quadrature value

v - velocity

w - intensity

D - flexural rigidity

E - Youngs Modulus

F - Force

$G()$ - Cross Spectral Density

G_{12} - Cross Spectral Density between signals 1 and 2

G_{ff} - Auto Spectral Density of f

H_{12} - Frequency response between signals 1 and 2

I - Second Moment of Inertia

L - length of beam

$J(x,t) or J(x,f)$ - Longitudinal Power Flow

M - Moment

P_B - Power of Flexural Wave

P_L - Power of Longitudinal Wave

Q - Shear Force

S - Cross Sectional Area

Δ - distance between measurement points

υ - poissons ratio

η - damping loss factor

θ - rotation

ϕ - phase difference between sensors (or channels)

ε - error due to finite difference approximations

ε_b - bias error

ξ - displacement (out of plane)

ς - displacement (in plane)

κ - radius of gyration

ω - radian frequency

$\Re\{\}$ - Real Part of

$\Im\{\}$ - Imaginary Part of

$\langle\ \rangle_t$ - time average

THIS PAGE INTENTIONALLY LEFT BLANK

Abstract

A method for the simultaneous measurement of both longitudinal and flexural wave intensities in beams is developed and measurements are then conducted on three specimens: a straight beam, a continuous T-beam, and a bolted T-beam. The work demonstrates that discontinuities in structures help to interchange large amounts of power between the two wave types. The straight beam serves to validate the measurement techniques. Successful comparisons are made to predicted power levels on a finite element model of the T-beam . The bolted T-beam shows the power flow is reduced across the bolted joint when compared to the continuous T-beam. The validated experimental results will form the basis for the validation of techniques (to be developed) to measure as well as calculate structural intensity in the presence of longitudinal and flexural waves.

Administrative Information

The work reported here has been funded by the Office of Naval Research, Code 0233, under program element 0602323N, in FY 95 and 96. A portion of the work was performed by the Applied Research Laboratory, at the Pennsylvania State University.

Introduction

An understanding of the vibration intensity patterns in a structure can aid in the identification of sources of high vibration levels, as well as permit the design of efficient and appropriate treatments or other structural modifications to control the vibration. For the last 25 years, the ability to determine these intensity patterns has been developing. For the most part however, the work is either limited to quasi-ideal structures, where only one wave type (such as flexural, bending, longitudinal, torsionsal, etc...) will exist, or it is assumed that the power is carried by one wave type. Structures of practical interest rarely have the luxury of a single wave type present at all frequencies, and therefore, unquantified errors begin to influence the measured power flow when only one wave type is measured.

Vibration damping treatments typically consist of tuned dampers, or a free or constrained viscoelastic layer. These treatments are most effective in damping flexural vibrations. If a significant amount of power is carried by longitudinal waves, the applied treatments will be largely ineffective in reducing the vibration levels. Even worse, the untreated longitudinal wave can interact with a discontinuity of some sort, and be converted to flexural waves with transverse displacements that generate acoustic pressures in the surrounding fluid. Thus, the longitudinal wave can act as a source of flexural vibration. To accurately determine the vibration power at a particular point on an object, it is necessary to know the amount of power flow which is due to every wave type.

The majority of the experimental work to date in the measurement of structural intensity has been concerned with flexural vibration in the near and far fields of discontinuities. Several experimental approaches have been explored since Noiseaux (1970) published expressions for the experimental determination of structural intensity in flexural waves. The power carried by longitudinal waves has been discussed by several authors, but experimental validation of proposed techniques is surprisingly hard to locate. Only in the work of McDevitt et.al. (1994) has longitudinal power flow measurements been validated

Considering all wavetypes in experimentally measured powers is difficult, since the full motion of a structure must be derived from only surface vibrations. In finite element models however, the complete vibration field of a structure is possible to calculate. Structure-borne powers

carried by flexural, longitudinal, and torsional wavetypes may then be calculated from the vibration field.

Such finite element power flow predictions may be made using the NSWCCD developed program McPOW (Mechanical POWer) , Hambric (1990A), a post-processor for the widely used finite element program NASTRAN (1986). McPOW has been applied successfully to many applications, including validation studies on a straight beam terminated with mounts (Hambric & Taylor 1994) and the Lexan T-shaped beam discussed in this report (Hambric, 1995). Also, an earlier McPOW study of a beam with several bends (Hambric, 1990) showed the importance of considering all relevant wavetypes in structure-borne power analysis.

McPOW will be used here to provide a database of spatially varying longitudinal and flexural powers against which the experimental results will be compared. Using finite element and experimental methods to investigate coupled longitudinal and flexural structure-borne powers will serve to validate both methods.

The purpose of the work reported here is to develop a methodology for and to obtain longitudinal and flexural power flow data on three structures: a straight beam, a bolted T beam, and a continuous T beam. These data will serve to demonstrate the need to measure both wave types on structures. In most previous work it is assumed that the power is carried only by flexural waves. Here, experimental confirmation of the theoretical predictions of coupling between bending and longitudinal waves at discontinuities in structures is obtained. In this report, results from measurements taken on both sides of the beams are presented. However, both sides of a structure are often not accessible, Therefore, the data obtained in this report will also serve as a validation for a future effort to develop a simpler method to determine longitudinal and flexural power flow simultaneously from measurements conducted only on one side of a structure. In this report, the history of structural intensity measurement techniques will be presented and will form the basis for understanding the expressions used in the later experimental work.

EXPERIMENTAL BACKGROUND

The mechanisms by which flexural and longitudinal waves in beams carry power have been described by Cremer, Heckl and Ungar (1966). However, the ability to measure these components did not begin until Noiseaux (1970) derived expressions to simplify the measurement of intensity in bending waves in the far field.

In the published works, the quantity of interest appeared to oscillate between Intensity and Power Flow. The two quantities are related. Intensity is the power flow per unit area.

It is well known that the transverse vibration of a beam can be described by the fourth order Helmholtz equation, $\frac{\partial^4 \tilde{\xi}}{\partial x^4} - k^4 \tilde{\xi} = 0$, where ξ is the out of plane (transverse) displacement and 'k' is the wave number. A solution to this equation is $\tilde{\xi} = A_+ e^{-jkx} + B_+ e^{-kx} + A_- e^{jkx} + B_- e^{kx}$. Notice that two of the exponentials, those following the B_+ and B_- terms are for non-propagating waves with amplitudes that decay exponentially. Thus, they are said to exist only in the 'near field'. Therefore, the 'near field' solution consists of all four terms, while the 'far field' (propagating) solution consists only of the two terms following the A_+ and A_-.

Noiseaux worked in the time domain. His experimental verifications were only performed in the far field, and required rotational and transverse acceleration measurements, as well as measurements of the strain.

Noiseaux used well known expressions to relate the shear force in a beam, Q_x, and the moment per unit width of the cross section, M_x, to the flexural displacement as:

$$M_x = -D\left(\frac{\partial^2 \xi}{\partial x^2} + \upsilon \frac{\partial^2 \xi}{\partial y^2}\right) \tag{1}$$

$$Q_x = -D\frac{\partial}{\partial x}\left(\frac{\partial^2 \xi}{\partial x^2} + \frac{\partial^2 \xi}{\partial y^2}\right) \tag{2}$$

where $D = EI/(1-\upsilon^2)$ is the flexural stiffness and υ is the poissons ratio.

Using the relationship between the rotation of the section and the flexural displacement as:

$$\theta = -\left(\frac{\partial}{\partial x}\right)\xi. \tag{3}$$

Noiseaux concludes that the intensity through a cross section of a beam is:

$$w_x = \left\langle Q_x \dot{\xi} \right\rangle_t + \left\langle M_x \dot{\theta} \right\rangle_t, \tag{4}$$

which is seen to be the sum of the force and moment components of intensity. The dot indicates a time derivative. Noiseaux also included a twisting moment component of intensity. Because of our restricted interest in this work to beams, we are ignoring the twisting component, which is typically more of a concern on plate-like structures. He also used free wavenumbers to remove the third derivative, so that he only had to measure displacement and slope.

Noiseaux also demonstrated that in the far field, the time averaged shear force and bending moment components of the structural intensity are equal. Consequently, only one of these components needs to be determined to know the far field flexural intensity.

Pavic (1976) extended the work of Noiseaux by developing expressions for the power flow of flexural vibration in the near and far fields which required knowledge of only the transverse displacement or velocity. Thus, he eliminated the need for the direct measurement of the rotation of a beam cross section. This was accomplished by relating the forces and moments which accompany flexural vibration to the first, second, and third order spatial derivatives of the structural transverse displacement, and relying on finite difference approximations and arrays of velocity or displacement sensors to obtain the higher order derivatives. Although all of his work was performed in the time domain, Pavic introduced the possibility of working in the frequency domain. Pavic ignores the twisting moment component of intensity, and began with the expression from Noiseaux above, [equation (4)], which he re-writes by noting that the shear force, $Q_x = \frac{D}{j\omega}\left(\frac{\partial^3 \xi}{\partial x^3}\right)$ and the bending moment $M_x = -\left(\frac{D}{j\omega}\right)\left(\frac{\partial^2 \xi}{\partial x^2}\right)$ and concludes that the flexural intensity can be described as :

$$w_x = D\left[\left(\frac{\partial^3 \xi}{\partial x^3}\right)\frac{\partial \xi}{\partial t} - \left(\frac{\partial^2 \xi}{\partial x^2}\right)\frac{\partial^2 \xi}{\partial t \partial x}\right] \tag{5}$$

This equation can be more simply applied to the determination of far field power if the Noiseaux conclusions that the power flow due to the bending moment and shear force are equivalent in the far field. In this case, only a single term needs to be evaluated. Equation 5 determines the power flow in the near-field of discontinuities if both terms are evaluated.

In order to obtain the spatial derivatives, he uses finite difference approximations and a co-linear array of four velocity transducers. The array is depicted in figure (1). Carefully note the order of the sensors, in which the first sensor location exposed to the flexural wave is number 4.

The finite difference approximations for the spatial derivatives needed in Pavic's intensity expression are (Timoshenko (1951)):

$$\begin{aligned}
\xi &\approx \frac{1}{2}(\xi_2 + \xi_3) \\
\frac{\partial \xi}{\partial x} &\approx \frac{1}{\Delta}(\xi_2 - \xi_3) \\
\frac{\partial^2 \xi}{\partial x^2} &\approx \frac{1}{2\Delta^2}(\xi_1 - \xi_2 - \xi_3 + \xi_4) \\
\frac{\partial^3 \xi}{\partial x^3} &\approx \frac{1}{\Delta^3}(\xi_1 - 3\xi_2 + 3\xi_3 - \xi_4)
\end{aligned} \tag{6}$$

where Δ is the spacing between measurement points. The power flow levels are determined at the middle of the array, one-half of the way between locations 2 and 3.

The error in the finite difference approximations has been quantified by Seybert (1981) among others, and are seen to be a function of frequency and measurement spacing.

$$\varepsilon = \frac{\sin(k\Delta)}{k\Delta}. \tag{6a}$$

The errors due to the finite difference approximations are corrected by multiplying the resultant power by the reciprocal of this error expression. Using the finite difference approximations in the intensity expression in equation 5, Pavic constructs the following expression for the instantaneous flexural intensity:

$$w_x \approx \frac{D}{\Delta^3}\left[\dot{\xi}_3 \int \left(\dot{\xi}_1 - 2\dot{\xi}_2 + \dot{\xi}_3\right) dt - \dot{\xi}_2 \int \left(\dot{\xi}_2 - 2\dot{\xi}_3 + \dot{\xi}_4\right) dt\right] \tag{7}$$

The time averaged near field flexural intensity is then presented as:

$$\langle w \rangle_t \approx \frac{D}{\Delta^3}\left[\dot{\xi}_2(4\xi_3 - \xi_4) - \dot{\xi}_1 \xi_3\right] \tag{8}$$

Thus, the flexural intensity at a point is now expressed in terms of the out of plane velocities and displacements of a series of points along a line.

Pavic then uses this expression, along with an analog circuit consisting of multipliers, inverting summers, inverting integrators, and averagers to determine the intensity at a point. He does not explicitly correct for the errors which are introduced by the finite difference approximations.

Although the experimental setup detailed by Pavic considers only time domain analysis, he introduces the possibility of frequency domain analysis through the use of a Fourier transform technique. If the displacement of the flexural wave is expressed in terms of the spectral density of the amplitude, as:

$$\xi(x,t) = \int_0^\infty \Re\left\{\left[\bar{A}_+ \exp(-ikx) + \bar{A}_- \exp(ikx)\right]\exp(i2\pi ft)\right\} df \tag{9}$$

then the Fourier transform of the displacement is related to the spectral density as

$$\bar{\xi}(x,f) = \frac{1}{2}\left[\bar{A}_+ \exp(-ikx) + \bar{A}_- \exp(ikx)\right] \tag{10}$$

Using these expressions in his original expression for intensity, eq 8, as well as the finite difference expressions, eq 6, Pavic derives the following expressions for the average far field flexural intensity:

$$\langle w \rangle_t \cong 2\frac{\sqrt{Dm}}{\Delta}\left\langle \dot{\xi}_1(t)\dot{\xi}_{2q}(t)\right\rangle_t \tag{11}$$

where the 'q' subscript refers to the quadrature value, which is the time signal that has been adjusted with a -90 deg phase shift to the signal. This 90 degree phase shift can be obtained by multiplying the Fourier transform by -i, and inverse transforming back into the time domain, or simply by applying an electronic phase shift if that option is available.

Verheij (1980) described how the frequency domain could be exploited using cross spectral density measurements to measure the flexural vibration of beams and plates, as well as the longitudinal vibrations of beams, and the torsional vibrations of pipes. This was an expansion of work presented by Fahy (1969,1977) where it was shown that vibration power flow can be determined from the cross spectrum between a force signal and an acceleration signal. No attempt was made in Verheij's work to demonstrate an experimental validation of the espoused approaches.

Verheij demonstrates that the time average product of two time varying signals can be obtained from their cross spectral densities, such that

$$\langle xy \rangle_t = \langle yx \rangle_t = \frac{1}{2}\Re\{\bar{X}^*\bar{Y}\} = \int_0^\infty \Re\{G(x,y,f)df$$

Using expressions from a table of equivalent signal processing operations in his paper, he expresses the far field power flow , $\langle P_b \rangle_t$, based upon the flexural intensity expression of Pavic as

$$\langle P_B \rangle_t \cong 2\frac{\sqrt{Dm'}}{\Delta}\int_0^\infty \frac{\Im\left\{G\left(\ddot{\xi}_2, \ddot{\xi}_1, f\right)\right\}}{\omega^2} df \qquad (12)$$

where the double dot notation indicates a second order time derivative, and m' is the mass per unit length.

Verheij also presents an expression for measuring the power flow in longitudinal waves on a beam, using finite difference approximations. Without presenting the derivation, he expresses the longitudinal power flow as a product of the force and in-plane velocity.

$$\langle P_L \rangle_t = \left\langle F\frac{\partial \varsigma}{\partial t}\right\rangle_t = -SE\left\langle \frac{\partial^2 \varsigma}{\partial t \partial x}\right\rangle_t \qquad (13)$$

where F is the in-plane force, ς is the in-plane displacement, and the convention of a negative force as tensile is adopted. Using finite difference approximations, and working in the frequency domain, he concludes that the longitudinal power flow can be determined from the following expression:

$$\langle P_L \rangle_t \cong -\frac{SE}{\Delta}\int_0^\infty \frac{\Im G\left(\ddot{\varsigma}_2, \ddot{\varsigma}_1, f\right)}{\omega^3} df \qquad (14)$$

The expression is not validated with experimental data, but Verheij proposes that the longitudinal acceleration can be obtained from the average of two accelerometers which are oriented to directly measure the in-plane acceleration on opposite sides of the beam, so that the accelerometers measure the longitudinal acceleration, while canceling out the flexural acceleration. This measurement approach results from the fact that for quasi-longitudinal vibration (using the terminology of Cremer et. al.), opposite sides of a uniformly thick beam will move in phase with each other. The component of vibration normal to the plane of the surface alternately contracts and expands due to the poisson effect and the traveling longitudinal wave. For flexural, or bending vibration, opposite sides of the uniformly thick beam are displaced 180 degrees out of phase with respect to each other. When longitudinal and flexural waves coexist on a beam, the surface displacements on either side are a combination of the effects of the longitudinal waves, and the flexural waves. The longitudinal component of the total vibration can be separated by averaging the measured displacements (or velocities or accelerations), from directly opposite sides of the beam. The flexural component can be obtained by subtracting the displacements from directly opposite sides of the beam.

If F_t is the flexural vibration on the top surface, and F_b is the flexural wave induced vibration on the bottom, then $F_t = F_b \exp(j\pi) = -F_b$. Similarly, let L_t and L_b be the surface displacement induced by the longitudinal vibration on the top and bottom surfaces respectively. Then from above, $L_t = L_b$. Any measurement of the vibration on either surface would measure the combined displacements of the two wave types. Thus, the total displacement measured on the top, T, would equal $F_t + L_t$. On the bottom, the measured displacement , B, would be $F_b + L_b$.

Verheij uses the average of the top and bottom measurements to obtain the longitudinal wave displacement. This is seen from:

$$\frac{1}{2}(T+B) = \frac{1}{2}(F_t + L_t + F_b + L_b) = \frac{1}{2}(F_t + L_t + (-F_t) + L_b) = L_t$$

Similarly, one half of the difference of the top and bottom measurements provides the flexural component:

$$\frac{1}{2}(T-B)=\frac{1}{2}(F_t+L_t-F_b-L_b)=\frac{1}{2}(F_t+L_t-(-F_t)-L_t)=F_t$$

Linjama (1989) expanded the work of Verheij , when he demonstrated useful experimental techniques to measure the near and far field flexural vibration of a thin beam. Linjama's work relies on an expression from Bendat and Piersol (1986), which permits the cross spectral density between two vibration sensors to be obtained by a series of frequency response measurements between each of the vibration sensors, and a reference signal, which might be a force gauge, or another vibration sensor.

The key relationship employed in Linjama's analysis is the description of the cross spectral density between the output of two sensors, at positions 1 and 2, as the product of the frequency response between the sensor at 1 and a reference sensor, the sensor at 2 and the reference sensor, and the power spectrum of the reference sensor, which is selected in this example (and also in the new work reported in this paper) as the force:

$$\hat{G}_{12}=H_{f1}^{*}H_{f2}G_{ff} \tag{15}$$

The caret indicates that the quantity is an estimated quantity. The repeated subscripts indicate an auto spectral density, as opposed to a cross spectral density which is indicated by the non-repeating subscripts. The * indicates a complex conjugate. The use of this relationship greatly simplifies the measurement of structure borne power flow for the case where the input force is stationary because the instrumentation requirements are now simplified to a two channel dynamic signal analyzer. If the same sensor is used for the measurement at position 1 and 2, then phase variability between sensors is also no longer a concern. Linjama presents expressions for both the near field and far field flexural wave power which are based upon the above expression.

In the far field case he concludes that:

$$P_B=2(\sqrt{Dm'}/\Delta)\Im\{\hat{G}_{12}\} \tag{16}$$

and in the near field case he concludes that:

$$P_B=\left(D/d^3\omega^3\right)\Im\{G_p\} \tag{17}$$

where $\hat{G}_p=\left(4H_{F2}^{*}H_{F3}-H_{F1}^{*}H_{F3}-H_{F2}^{*}H_{F4}\right)G_{FF}$ (18)

and the order of the sensors is consistent with that of Pavic (1976) as shown in figure 1, that is, the flexural wave arrives at sensor 4 first, and then 3,2,1 respectively.

Equations (16) and (17) are valid only when the measured quantity is acceleration, and the reference signal is a force. Linjama's equations assume slightly different forms if the measured quantity is a velocity or a displacement, and if the reference is something other than the force.

Linjama presents experimental data of the measured flexural power flow in a long thin beam driven at one end, and damped at the other. He determines the power at a single point in the

center of the beam using the far-field measurement technique as well as the near field measurement technique and the agreement was seen to be very good. Linjama's expressions are not explicitly corrected for finite difference errors.

Errors which are introduced in the determination of flexural power flow other than finite difference errors were analyzed by Carroll (1987). He concluded that although the finite difference errors themselves were minimized when the spacings were as small as possible, the bias errors (due to the standing waves present on a finite length beam) in the experimentally determined power flows were minimized when the spacings were at 1/4 wavelength. Standing waves can obscure the measurement of the traveling waves which carry the power. Power is not carried by a standing wave. The measured velocities in a beam which has standing and propagating waves are the sum of the velocities of both the propagating and standing waves. Similarly, the phase relationship between any two points on a beam due to the traveling wave is mired in the standing wave phase relationship. Carroll shows that the bias error due to the standing wave can be expressed as

$$\varepsilon_b = \frac{2(\phi)\cot(k\Delta)}{Lk\eta}$$

where ϕ is the phase difference between measurement channels, 'L' is the length of the beam, and η is the damping loss factor of the structure. The bias error is clearly minimized when the spacing equals a quarter wavelength, because here, the product $k\Delta = \frac{\pi}{2}$, and $\cot\left(\frac{\pi}{2}\right) = 0$. Although the use of a quarter wave spacing results in a large finite difference error (a factor of 1.57), this error is quantifiable, as has been shown, and therefore, the resultant power flow can be corrected using the reciprocal of equation 6a.

The advantage of Linjama's method for using a single transducer is also demonstrated by the above description of the bias error. The phase differences, ϕ , due to difference transducers is eliminated. Some phase differences still remain, due to phase drift in the sensor and the electronics, but with typical commercially available equipment, these values are small. Some low end accelerometers are known to have problems with phase drift, and these should obviously be avoided.

Baker et.al. (1989) presented an expansion of the frequency domain analysis of the work of Pavic (1976) for longitudinal power flow in a beam of uniform cross section. No experimental validation is presented by Baker et.al. Fundamentally, the representation for the power flow due to in-plane waves is similar to that presented by Verheij. However, whereas Verheij recommended the measurement of the longitudinal acceleration with accelerometers which are placed on their sides and on opposing sides of a structure, equations presented by Baker et.al. allow for the accelerometers to be placed normal to the beam surface. They reason that because an applied longitudinal stress will produce a lateral strain, equal to the product of the Poisson's ratio, and the longitudinal strain, that it is sufficient to measure the normal (lateral) strain and calculate the longitudinal stress. He concludes that flexural and longitudinal Power can be obtained from the same generalized equation,

$$\langle P \rangle = C\left\langle (a_2 - a_1)(a_{2(q)} + a_{1(q)}) \right\rangle \qquad (19)$$

where for longitudinal power flow measurements,

$$a_1 = a_{1T} + a_{1B}; a_2 = a_{2T} + a_{2B}; C = \frac{ES\upsilon^2}{8\omega^3\Delta} \qquad (20)$$

and for flexural power flow measurements,

$$a_1 = a_{1T} - a_{1B}; a_2 = a_{2T} - a_{2B}; C = \frac{\sqrt{mEI}}{4\omega^2\Delta} \qquad (21)$$

where a_{xx} represents an acceleration at 1T (position 1 on top of the beam), 1T (position 1 on the bottom of the beam), etc...

Although Baker et.al. use the quadrature notation, these expressions can be re-written into an alternate notation which employs the cross spectral density to determine the power flow, and the result is identical to the expression for longitudinal and flexural power flow found in Verheij (1980), with the exception of the Poisson ratio term. The expressions of Baker et.al., in either the quadrature or cross spectral density form, are convenient because they allow for the simultaneous determination of the two wave types, provided that the structure is uniformly thick, and you have access to both sides.

The implementation of the Baker et.al. expressions, as presented, require four phase matched accelerometers, and a four channel signal analyzer.

Horner and White (1990) present the first longitudinal power flow data that is known to this author. The expressions are based largely upon those of Baker et.al. (1989) Although the introduction claims that the paper will demonstrate a method to account for standing waves and unwanted waves (for example, longitudinal waves are unwanted if one wishes to know the flexural wave power), the data presented is in a limited frequency region (90 Hz wide) where the authors claim that the beam exhibits "infinite" behavior. The measured accelerance is flat in this region, giving rise to the claim that there are no reflected waves - thus, the beam appears to be infinite. The measured power in the beam, normalized by the input power, does not match the values predicted by the authors. They attribute this discrepancy to the poor flexural wave attenuation in the beams. (Although Horner and White claim that their results are incorrect , this work of Horner and White is included here because it is the first to include longitudinal power flow data.)

In the only other presentation of longitudinal intensity data that has been identified, McDevitt et.al. (1993,1994) present approaches to measure flexural and longitudinal intensity in a beam using a two channel laser velocimeter. The two laser beams are focused on two closely spaced points, and determine the in-plane velocity at these points. The principles of Verheij, as well as finite difference approximations are used to calculate the longitudinal power flow at a point half way between the points illuminated with the two laser beams.

The measured longitudinal power flow is corrected for finite difference errors, and is validated by comparing the results to those obtained by the standing wave and energetics methods, which are detailed by Carroll (1987). The good agreement between the three approaches validates both the laser measurement approach of McDevitt et.al., as well as the longitudinal power expressions of Verheij. The disadvantage of the measurement approach of McDevitt is that flexural waves contaminate the measured in-plane velocities. The method that McDevitt used was not used to discriminate between the various mechanisms for power flow in a structure.

VALIDATION STUDIES

The measurement of flexural power flow on straight beams appears to be well known, with validated data found in the literature [Linjama(1992), Hambric and Taylor (1995)]. McDevitt (1994) demonstrates that the longitudinal power flow expressions on a straight beam are also valid. In the experimental part of the work presented herein, we seek to demonstrate that the longitudinal power flow can be extracted from a vibration field which also has a flexural power flow component by using a combination of the results of Linjama and Verheij. The combination of methods results in a relatively simple measurement procedure that requires only a minimum of test equipment. Furthermore, we wish to expand beyond a simple beam into an intersection of beams in the shape of a T. With this T-shaped beam, we are forced to include the flexural near field power flow, as well as the longitudinal power flow, as it is expected that some portion of the flexural wave will be converted to a longitudinal wave in the presence of the junction, and vice versa.

For the purposes of developing and evaluating the techniques to measure as well as calculate longitudinal and flexural power flow along beams, three structures were constructed and evaluated.

- Description of the Beams

The three structures which are evaluated in this work are 1- a straight beam, 2- a continuous T beam, and 3 - a bolted T beam. They are all constructed from the same sample of a thermoplastic material, which was chosen over metal primarily for the high material damping which reduced the amplitude of the standing waves relative to the amplitude of the propagating waves. The higher damping levels are also considered to be desireable because of the dissipation of the power that would occur as the vibrations traveled along the beam. As a result of this dissipation, the measured and predicted power levels will be a function of position in the beam. This will provide a more rigorous comparison of the experimental and predicted power flow. With low damping, standing waves occur, and power will not flow. The product Zelux M® was chosen because it is annealed in the fabrication process, which made it easier to machine, and more resistant to chipping, splitting, or breaking.

The straight beam is 73.25 inches long. This is also the dimension of the longest leg of the T beam. The third leg of the T-beam is 36 inches. The experimental setup is shown in the photograph in figure 2. The cross sectional dimensions of all of the parts are 1.25 inches x 2.125 inches.

For all measurements, the beams were suspended at each end by resting the 1.25 inches side on a suspension bridge composed of a wire span held up by springs, as shown in figure 3.

A three point flexural test on the beam material determined that the Young's modulus of the material is 2.62×10^9 N/m^2 ,(std dev 1%).[1] The density was measured to be 1239.56 kg/m^3 . These data suggest a longitudinal phase speed of 1453.84 m/s , using the relationship $c = \sqrt{E/\rho}$. A simple test suggests that this number appears to have some error. The calculated phase speed is used in the computation for the flexural resonances of a free-free beam, $f = \frac{\pi c \kappa}{8L^2}(3.0112^2, 5^2, 7^2, \ldots)$ and these calculated values are compared in table 1 to the actual

[1]Measured in the Plastics and Rubber Branch, Carderock Division, NSWC, Annapolis Det.

measured resonances. The measured values are seen to be approximately 8% lower than the calculated resonances.

The calculated phase speed is also used in the computation for the longitudinal resonances of the free-free beam, $f_n = \frac{nc}{2L}$, and these calculated values are compared in table 2 to the actual measured resonances. The measured values are seen to be approximately 4% higher than the calculated resonances.

Calculated Resonance	Measured Resonance	% difference
13.86	12.8	-7.6
38.5	35.3	-8.3
75.46	71.8	-4.8
124.7	116.3	-6.7
186.3	170.94	-8.2
260.26	241.25	-7.3
346.5	318	-8.2
445	405	-8.9
556	504	-9.3

Table 1: FLEXURAL RESONANCES OF Free-Free STRAIGHT BEAM

Calculated Resonance	Measured Resonance	% difference
361.72	377	4.2
723.44	750	3.67
1085.26	1125	3.66
1446.88	1510	4.36
1808.6	1880	3.95

Table 2: LONGITUDINAL RESONANCES OF Free-Free STRAIGHT BEAM

The differences between the measured and calculated resonance frequencies can be attributable to either boundary conditions which are not ideally free-free, or error in the Youngs modulus or density measurements. Errors in the Youngs Modulus or Density would result in comparisons for the longitudinal and flexural waves which are either both high or both low. Since the measured flexural resonances are higher than the calculated values, and the measured longitudinal resonances are lower than the calculated values, it is not likely that the cause of the discrepancy can be traced to material property errors. If either end of the beam were fixed, the calculated resonances would be lower than the frequencies calculated for a free-free beam. This is potentially the cause of the discrepancy, at least for the flexural resonances. Because the measured longitudinal resonances are high, a situation which is unexplainable due to boundary condition differences, it is possible that the measured modulus and density does contain an error. Assume that the calculated longitudinal phase speed is 4 % too high due to material property data errors. If a reduced wave speed, equal to 96% of the initial wave speed (or 1394 m/s) is assumed, then the calculated flexural resonances are within 5% of the measured values, a difference which may be attributable to boundary conditions.

It seems reasonable to think that the differences between the measured and calculated resonances are the result of a combination of errors: non-ideal boundary conditions, as well as in-exact values of the Youngs Modulus and density. For the purposes of the power flow measurements, the differences mentioned above are relevant because the longitudinal power flow is proportional to the Youngs Modulus and the flexural power flow is proportional to the square root of the Youngs Modulus and the density. The finite element predictions of resonances and power levels also require knowledge of the Young's Modulus and density. Thus, these differences could be used to explain any differences in the final comparisons between the measurements and the predictions.

The bolted T-beam is assembled by bolting through the long span, with two 1/4 bolts, into

> The loss factor of the beam materials was measured using the half power point method, when subject to both in-plane and flexural excitation. The measured loss factors are fairly independent of frequency, and are approximately 0.01, (Q=100). The loss factor data are plotted in figure 4.

helicoils inserted into the end of the 36 inches beam.

- Experimental Approach

Using a combination of the work developed by Linjama (1992) and Verheij (1980), a set of equations have been developed which permit the calculation of flexural and longitudinal power flow at points along the beams, after the collection of frequency response data between one of the force gauges, and a single roaming accelerometer. These frequency responses are collected on both sides of the beams.

Although it is desirable to make a single measurement at each point in order to obtain both the longitudinal and flexural power flow, as described by Baker(1989), it was not possible in this series of experiments to extract the longitudinal component of the traveling wave by measuring only the velocity differences parallel to the surface which resulted from the Poisson contraction and expansion when a longitudinal wave passes the measurement point. It was necessary, for all measurements on the three beams of this series of experiments, to measure the normal component of acceleration on two sides of the beam in order to determine the flexural wave power flow. It was further necessary to measure the axial (or in-plane) acceleration on both sides of the beam to determine the longitudinal wave power flow.

The measurement approach of Baker(1989) requires the extraction of the longitudinal component by adding the measured accelerations from opposite sides of the beam, thus canceling out the flexural wave components. The Poisson displacement is typically very small relative to the flexural wave displacement, and consequently it can be difficult to extract the Poisson displacement. Minor errors in locating the opposing sides of the beam can result in the large errors in the apparent Poisson displacement, especially as the wavelength decreases. Similarly, equipment noise can be high enough that the very small poisson displacement is of a comparable level, especially if the measurement transducers are not very sensitive.

Fortunately, the measurement process allows one to determine the quality of the data. Because the frequency response between the drive force and the acceleration is measured, the magnitude of the frequency responses can be plotted at a single frequency as a function of position along the beam. This plot is the mode shape of the beam at the selected frequency. If the resultant plot has the period of a longitudinal wave, then the data acquired is acceptable for power flow calculations. If the data is not usable, it has the appearance of random noise rather than a longitudinal wave mode shape. (The same procedure is used to determine the quality of the

flexural wave.)Unfortunately, this was the typical result in these experiments. Thus, a second measurement at each point was required. For this measurement, the in-plane acceleration is measured directly. By addition of the acceleration on the opposite sides of the beam, any potential flexural component is eliminated. With this configuration, it is the flexural component which is small relative to the longitudinal component, and the measurement of longitudinal data is then forgiving to small errors in placement. As before, a simple plot of the magnitudes of the frequency response at a frequency as a function of position along the beam is a good test of the quality of this data.

A second feature of the examination of the mode shape is that the quarter wavelength is immediately obvious. Thus, the proper spacing for the minimization of standing wave induced bias errors is determined without any apriori calculations or knowledge of the beam material properties.

The force is monitored and stored for later analysis in order to verify that the force levels are stable. This monitoring is necessary in order to validate the requirement that the force remain constant throughout the experiment. The force is also used for comparison to other data sets, because the power levels can be normalized to the input force.

Regardless of which beam is being tested, and whether the force is applied axially or transversely, the following steps are taken in the collection of the data:

Initially, the input power is determined from the cross spectra between the force gauge which is located between the shaker and the beam and an accelerometer which is at the location of the applied force, using:

$$P_{in} = \frac{2}{\omega}\Im\{G(F,a,f)\} \qquad (22)$$

Two force gauges are used. When the force gauges have the same output reading, it is considered that minimal twisting moment exists in the forced excitation of the beam. Because of our use of only a two channel signal analyzer, only one of the force gauges can be used in the computation of the frequency response. One consequence of the use of the two force gauges is that the gauge which is used to measure the input power only determines 1/2 of the input power. Therefore, the factor of 2 in the numerator accounts for the fact that the single force gauge measures only half of the input force.

The same accelerometer is then moved down the length of the beam. At constant intervals, the frequency response between the acceleration and the applied force is measured on both sides of the beam. Every time the frequency response is measured, the input force is also separately measured.

The frequency response measurements from both sides of the beam are then combined. To determine the effective flexural wave frequency response at position 1:

$$H_{a1} = \left[\left(H_{1Ftop} - H_{1Fbot}\right)\right]/2 \qquad (23)$$

To determine the longitudinal wave frequency response at position 1:

$$H_{a1} = \left[\left((H_{1Ftop}) + (H_{1Fbot})\right)\right]/2 \qquad (24)$$

The principles of Linjama are then used to calculate the near and far field flexural powers from the effective frequency responses just determined.

For the far field flexural power flow calculations, the cross spectra between two adjacent measurement points is determined from

$$G_{a1,a2} = H_{a1}^{*} H_{a2} G_{FF} \qquad (25)$$

The subscript on the cross spectra indicates the measurement point, again using Pavics convention, where point 2 comes before point 1.

The far field flexural power is then calculated from

$$P_{flex-ff} = 2(\sqrt{Dm} / \Delta)\Im\{G_{a1,a2}\} \qquad (26)$$

For the near field calculations, the cross spectra between four adjacent measurement points is

$$G_{a1a2a3a4} = \left(4H_{a2}^{*} H_{a3} - H_{a1}^{*} H_{a3} - H_{a2}^{*} H_{a4}\right) G_{FF} \qquad (27)$$

The near field flexural power is calculated from

$$P_{flex-nf} = \left(D / \Delta^{3} \omega^{3}\right)\Im\{G_{a1a2a3a4}\} \qquad (28)$$

The expression which is used to determine the longitudinal power is derived in appendix A. The resultant expression from this derivation is:

$$P_{longit} = J(x, f) = \frac{SE}{\Delta \omega^{3}} \Im\left(G_{a1,a3}\right) \qquad (29)$$

where the cross spectra which is appropriate for longitudinal power flow (from using equation 24 in equation 25) is selected. 'J' is the notation for the longitudinal power flow from Cremer et.al. (1966).

- Finite Element Approach:

Finite element methods for predicting structure-borne powers in beams have been developed and implemented in McPOW (Hambric 1990a). The methods have been validated in two prior studies, Hambric and Taylor, (1994) and Hambric (1995), and are summarixed here. A finite element beam model is comprised of many elements, each of which has two nodes. Complex velocities and forces at each node of a beam element are combined to compute the powers carried by all wavetypes:

$$Power = \Re\left(F_x v_x^{*} + V_y v_y^{*} + V_z v_z^{*} + M_y \dot{\theta}_y^{*} + M_z \dot{\theta}_z^{*} + T_y \dot{\theta}_x^{*}\right) \qquad (30)$$

where

F_x is the axial force;

V_y is the shear force in the y direction;

V_z is the shear force in the z direction;

M_y is the bending moment about y;

M_z is the bending moment about z;

T is the torque;

v_x^*, v_y^*, v_z^* are the complex conjugates of the translational velocities, and

$\dot{\theta}_x^*, \dot{\theta}_y^*, \dot{\theta}_z^*$ are the complex conjugates of rotational velocities.

The average of powers at each node is taken to find an element power. Mechanical intensities are simply the powers divided by the beam cross sectional areas.

The straight beam and the continuous T-beam were modeled using one inch elements, which gives a mesh density sufficient to resolve longitudinal and flexural waves for frequencies up to 1000 Hz. Since the excitation and response of the T-beam is planar (assumed to be the xy plane) for all cases considered in this report, powers are computed only for flexural waves in the plane of the T-beam and longitudinal waves:

$$Power = \Re\left(F_x v_x^* + V_y v_y^* + M_z \dot{\theta}_z^*\right) \tag{31}$$

where the flexural powers are the sum of the shear and moment terms.

To compare finite element and experimental results, the structure-borne powers are normalized to the input powers at each frequency of interest. Input powers are computed by McPOW as:

$$Power_{input} = \Re\left(F_{in} v_{in}^*\right) \tag{32}$$

where

F_{in} is the applied force, and

v_{in}^* is the complex conjugate of the velocity in the direction of the applied force.

- General Experimental Setup

For all three beams, the force is applied from a Wilcoxen Research F4 shaker, which is driven by random noise from 0-2000 Hz. The output of the shaker is connected to a stinger, which is then connected to a jig which consists of two PCB model 208B01 force gauges. The gauges measure the force at either end of the 2.125 dimension of the beam, The purpose of the two force gauges is to insure that the beam is driven normally, with minimal moment forces imparted by the force. The experiment proceeds only when the two gauges have the same reading. The force signals are amplified with a PCB model 483A signal conditioner. Acceleration is measured with Bruel and Kjaer model 4374 accelerometers, and amplified with a B&K model 2635 charge amplifier. All signals are monitored with an oscilloscope, and are analyzed with a Hewlett Packard 3562 Dynamic Signal Analyzer. The entire measurement process is controlled via a custom written LABVIEW Routine, which corrects all signals for gain and sensitivities, before storing the data to a Macintosh 540c. All subsequent data processing is performed within MATLAB.

Power flow plots will appear in the following format , for each condition being discussed. The structure borne power, in either the base beam or the stem will be plotted as a percentage of the input power. With the T-beams, the stem (leg B) is located 30 inches from the drive point. Therefore, the power levels in the stem are plotted on the same plot as the power in the base beam (legs A & C). On the plots, the stem powers begin to appear at an ordinate of 30 inches, because this is the distance from the drive where the stem begins. The predicted power levels (also normalized by the input force) will be plotted along with the measured levels also.

Straight Beam

The longitudinal wave and flexural wave power flow measurements on the straight beam were performed for the purposes of demonstrating the experimental techniques on as simple a structure as possible. With a straight beam, it is possible to generate either pure flexural waves, or pure longitudinal waves. The accuracy of the measurements can be assessed by comparing the measured input power with the measured structure-borne power on the beam near the drive. The two powers should agree with each other. Furthermore, the structure-borne power at the free end of the beam should approach zero. Finally, the dissipation of the flexural power along the length of the beam should be proportional to $\exp\left(\frac{-k_B \eta x}{2}\right)$, as derived in appendix B.

With the straight beam excited with the force applied normal to the surface of the beam, flexural waves are predominantly excited.

Figures 5 & 6 are the flexural and longitudinal input powers (per unit input force) for the straight beam.

There are differences between the measured and predicted resonances in both figures 5 and 6. This may be due to the uncertainties in the Youngs modulus and density as well as boundary conditions, as were discussed earlier. For the predictions, the beam is easily held in an ideal free-free manner. This is not so easy to do experimentally. Recall from the discussions of tables 1 and 2 that the boundary conditions were considered to depart from free free, and that errors were likely in the material properties.

The measured data also contains steep drop offs between the resonances, especially at the lower power levels. The cause of these drop offs is unknown, but the fact that they occur only at the lower power levels, and not at the higher ones suggests that they may be due to low signal levels in either the applied force, or the measured acceleration response. These differences will be discussed further later in this report.

Figure 7 is the measured and predicted structure borne power field at 420 Hz. a flexural resonance, for the flexural force input. In figure 7, observe that at the drive location, the flexural power is approximately 100 % of the input power. At the mid point on the beam, the power levels are reduced to 50%, and at the free end, the power approaches zero watts. This is a good check on the validity of the resultant power flow fields. The comparison between the measured and calculated flexural powers is good. The longitudinal power calculation is left off of the plot for clarity. In an analytical model, the input force can be directed to be purely flexural if that is desired. The longitudinal power would appropriately approach zero. In physical models, boundary conditions and alignment errors will exist. The measured longitudinal power levels are seen to be approximately at zero. The longitudinal power levels are plotted here to demonstrate the quality of the experimental setup.

Figure 8 shows the flexural and longitudinal powers respectively, measured at 780 Hz, a longitudinal resonance. For the same reasons that figure 7 did not contain the predicted longitudinal powers, figure 10 does not contain the predicted flexural powers. The low measured flexural powers, relative to the longitudinal powers again confirms the high quality of the experimental setup. With the exception of the data points around 50" from the drive, the comparison between the experimental and predicted longitudinal power is good. Although the fact that the two bad points are neighboring may suggest a pattern, it is likely that these two bad points are the result of a single bad data point. Recall that the power at one point requires measured acceleration at two points. Consequently, each measurement point contributes to the experimental power at two neighboring points. These bad data point may be due to a poor installation of the accelerometer, such as from a misalignment or a bad bond.

The measured input and structure borne powers for the flexural and longitudinal waves on the straight beam indicate that the measurement techniques and equations are correct and are being properly applied. With confidence, we progress to the T-beams.

Continuous T beam

The longitudinal and bending input admittances for each leg of the T beam were measured in order to understand the power flow fields that would be measured. If a wave is considered to originate at the tip of leg A (where the shaker will be located throughout these experiments), then the input admittance to the stem is at the base, where it intersects legs A and C, as opposed to the free end. Similarly, the input to leg C is not at its free end, but at the junction with the stem. The input admittances are determined with a drive point measurement of the force and acceleration in either the axial or normal directions at the locations described above. The longitudinal admittance to the stem is measured from the underside of the base beam, and normal admittances to legs B and C were measured 1" away from the junction. The only point which could not be obtained is the axial input to leg C. For this data, the longitudinal admittance at the free end is substituted. The normal and axial input admittances are plotted in figures 10a and 10b respectively. It is immediately obvious that all legs do not have resonances at the same frequencies.

- ---------- Axial Force applied to one leg of the T----

The continuous T beam was configured so that the force was always applied to the 30 inches leg (leg A) . In the first of the experiments performed, the force was oriented axially, so that longitudinal waves were predominantly excited in the 30 inches leg, figure 9a. In a subsequent test, the force was directed normal to the surface at the end of leg A, to excite flexural waves primarily, figure 9b.

The measured and predicted input axial power (normalized by the input force) is shown in figure 11. In general, the comparison is good. As was observed with the straight beam, the measured data contains steep drop offs between the resonances, especially at the lower power levels. (These drop offs were observed in all measured input powers.) The cause of these drop offs is unknown, but the fact that they occur only at the lower power levels, and not at the higher ones suggests that they may be due to low signal levels in either the applied force, or the measured acceleration response. Other experimental information suggests that they are due to low levels of the applied force. The drop offs change as a function of the force excitation hardware. When the stinger is removed from the path of the excitation force, the drop offs are minimized. In a previous paper discussing this T-beam , Hambric (1995) shows a much cleaner input power. In the experimental arrangement of that effort, a stinger was not employed between the shaker and the beam. It was decided to continue to use a stinger in these

experiments, because it was considered to be more important that the shaker not impart any moment or shearing forces to the beam.

In figures 12 and 13, the measured and predicted flexural and longitudinal powers are plotted for the base (legs A and B) and the stem (leg C) of the T-beam at 670 Hz, when the force is applied axially to the beam. At 670 Hz, the stem is at a longitudinal antiresonance, and leg C is at a relatively weak flexural resonance. The other legs are at longitudinal and flexural resonances. The flexural powers shown in figure 12 indicate that the power is approximately zero , and slightly negative (indicating power which is flowing towards the drive) along the base prior to the stem. However the stem has a much higher flexural power. The flexural power at the origin of the stem (where it intersects the base beam) is 40% of the input power. At first, it seems incorrect that the stem could be excited with 40% of the input power. How did this power travel to the stem when the base beam has no flexural power? It appears that the flexural vibration in the stem is caused by the longitudinal vibration in the base. Figure 13 shows that the longitudinal power in leg A is approximately 85% of the input power as it approaches the stem, and that it drops to 15% of the input power after it passes the stem, and enters leg C. The power drop can be explained by the power that was required to excite the flexural wave in the stem. The negative flexural powers in leg A mean that the flexural power is flowing towards the original source of the vibration. By associating the observed power levels with the locations of the resonances and antiresonances, it appears that power flows into the legs which are at resonances, regardless of whether it is a flexural or longitudinal resonance.

Observe that because the power in leg A is negative. This indicates that all flexural waves are traveling away from the junction.

Figures 14 and 15 are structure borne powers at 735 Hz. The power flow fields are qualitatively similar to the results in figures 12-13. The longitudinal wave is the source for the flexural waves at the position of the intersection, and the flexural waves are all flowing away from the junction. What is different at 735 Hz is that a relatively strong longitudinal wave is excited in the stem. In fact, this is the only frequency below 1000 Hz where a strong longitudinal mode was observed to be excited in the stem when the driving force was oriented axially. Because of the longitudinal mode in the stem, the flexural modes excited by the longitudinal mode which was incident upon the junction are all much weaker than observed at 670 Hz. In this case, the flexural powers in legs B and C are less than 5% of the drive power. As was observed at 670 Hz, all flexural powers are travelling away from the junction.

To summarize figures 12 through 15, the longitudinal wave initially excited in one leg of the T beam, traveled to the junction, where it excited flexural waves which traveled away from the junction in all three directions. At the junction, the power seemed to take the path of least resistance. That is, it traveled into a resonance (either flexural or longitudinal) in either receiving leg.

- ------- Flexural Force applied to one leg of the T---------

The continuous T beam was then configured so that the force was applied normal to the 2.125 inches surface of the 30 inches leg (leg A) . The point of application of the force was the end of the beam, as shown in figure 9b. Qualitatively, the results are similar to those seen above with the axial force. At some frequencies, the incoming flexural wave reaches the junction and

excites longitudinal waves that radiate away from the junction. The relative power in these longitudinal waves is less than those of the flexural waves created by the incident flexural waves. At some frequencies, the incident flexural wave travels to the junction, and splits its power among flexural waves in the two receiving branches. Thus, very little (if any) of the flexural power is converted to longitudinal vibration. The conversion to longitudinal waves appears to be less efficient than the conversion to flexural waves.

The measured and predicted input flexural power (normalized by the input force) is shown in figure 16. In general, the comparison is good. As was observed with the straight beam and the axial input to the continuous T, the measured data contains steep drop offs between the resonances, especially at the lower power levels.

Data is presented at the same two frequencies that were presented in the previous section, with an axial input force.

In figures 17 and 18, the incident flexural power at 670 Hz reaches the junction and excites longitudinal vibration in each of the three legs. This flexural vibration is seen in figure 18 to radiate away from the junction on every leg of the T beam. Approximate 30% of the flexural power that entered the junction continues through to the second half of the base beam as a flexural wave. Approximately 30% of the incident flexural power appears in the stem as a flexural wave. No significant longitudinal energy is generated at the junction. Note that there are also no strong resonances here. In contrast, legs B and C both have relatively strong flexural resonances.

At 735 Hz, a strong longitudinal resonance exists in the stem, and legs A and C are not at flexural resonances. Observe that this is consistant with the power flow. The input flexural wave travels to the junction, and 35% of that power travels into a longitudinal resonance in the stem, figure 20. This contrasts with the flexural power on the stem, which is not at a flexural resonace, and appears in figure 19 to have accepted very little power. Observe that at 735 Hz when the input is a flexural power, the longitudinal wave in each leg is travelling away from the junction. In the source leg, the longitudinal wave is travelling towards the source of the original vibration.

Bolted T beam

The experimental setup with the bolted T beam was designed to duplicate the measurements on the continuous T beam as closely as possible. The bolted T beam was configured so that the force was always applied to the 30 inches leg. In the first of the two experiments performed, the force was oriented in such a manner that longitudinal waves were predominantly excited in the 30 inches leg, as previously seen in figure 9a. Subsequently, the force was directed to apply flexural excitation primarily, as seen in figure 9b.

No finite element predictions were made for the bolted T beam.

- ------- Axial Force applied to one leg of the T---------

The structure borne power measurements on the axially driven bolted T beam are both qualitatively similar to the results observed with the continuous T beam. The axial power flow

that is incident on the joint is converted to flexural waves which radiate away from the joint in all three directions. The longitudinal power levels on the receiving legs of the joints tend to be low, indicating that a significant amount of the power is converted to flexural power. In contrast, when the vibration incident to the joint is flexural, the wave efficiently passes through the joint, with very little being converted to longitudinal power in either receiving leg. This is qualitatively similar to the results observed previously with the continuous beam. This indicates that the difference in these attachment methods, between the continuous and the bolted joints does not affect the mechanisms of power transmission and conversion across the joint. This can not be extrapolated to all junctions, as the power flow is likely to be a function of the quality of the attachment. What this shows is that a joint with well mated surfaces and tight bolts can act like a continuous connection.

In the first of the experiments performed, the force was oriented axially, so that longitudinal waves were predominantly excited in the 30 inches leg, figure 9a.

Observe in figure 20 that no significant longitudinal power has passed through the junction. As seen in the next figure, flexural power has been created on the far side of the intersection, as a consequence of the incident longitudinal wave.

Figures 21 and 22 contain the flexural and longitudinal wave powers at 735 Hz, with the force applied axially. This same frequency was plotted previously with the continuous beam. As seen at other frequencies on the bolted beam and on the continuous beam, the incident longitudinal wave excites flexural waves which radiate away from the junction on all three legs. As seen in figures 14 & 15 with the continuous beam, the stem has a large amount of longitudinal power. The trends between figures 14-15 and 21-22 are quite similar. This demonstrates that at least for these joints and beams, the power flow field through the junction was not dependent upon the construction.

- Discussion

Most reported measurements of structural power flow measure the flexural power flow exclusively. The reason cited is usually that the flexural waves have a much greater normal displacement, and therefore, produce greater acoustic radiation. While this may be true, a second reason may very well be that the methods to measure longitudinal wave power are not well developed. In fact, only one researcher , McDevitt et.al. (1994) reports measurement results of longitudinal power flows that were validated. The trouble with considering only the flexural power is threefold: the measured flexural powers will have an unknown amount of error, if the longitudinal power is unknown; the longitudinal wave can be a source for flexural waves, and therefore, the sudden appearance of flexural power in a beam will be unexplainable if the longitudinal power is unknown; and the longitudinal waves are faster than flexural waves. One consequence of faster longitudinal waves is that the longitudinal waves have a higher acoustic radiation efficiency than the flexural waves, even if the normal displacement amplitudes are lower than they are for the flexural wave. Consequently, radiation efficiency measurements based upon flexural wave measurements may be erroneous.

With the power flow measurement methods used in this report, the powers in longitudinal and flexural waves are determined. The technique is relatively simple and the instrumentation required is not highly specialized. It requires only a two channel dynamic signal analyzer, one accelerometer and one force gauge (or two accelerometers and no force gauge). The force gauge (or the second accelerometer) becomes a reference sensor, which is fixed for the length of the experiment. The other accelerometer is moved from point to point along the beam. By making two frequency response measurements between the reference sensor and the roaming

accelerometer on opposite sides of the beam the two wave components can be separated by either adding or subtracting the signals from each other, as described earlier.

An alternate approach is to use accelerometers oriented normal to the surface where the longitudinal component that is measured is the acceleration due to the Poisson effect. This can be a rather small value. To obtain the longitudinal component of power from a combination of flexural and longitudinal waves, one typically is trying to extract a small signal from a much larger one. Thus, the experimental technique has to be rather precise.

It is required to make measurements on exactly opposite sides of the beam. Small placement errors can introduce large errors in the determination of amplitudes associated with the wave type of interest. This is especially the case when trying to extract the longitudinal wave from a flexural/longitudinal combination, and especially at the higher frequencies, where the wavelengths get smaller.

For most of the measurements in this report, it was not possible to extract the longitudinal wave by measuring the normal acceleration. Although the reasons were not identified, small placement errors, as mentioned above may be the reason. It was considered at one point that the measuring accelerometer was not sensitive enough to measure the small poisson induced accelerations. However, measurements with more sensitive accelerometers also failed to separate the longitudinal component. A third possibility is simply the amplitude resolution of the dynamic signal analyzer, which is a function of the Analog-Digital Converter size. The normally oriented acceleration of the longitudinal wave can be viewed as a small addition / subtraction to the larger values of the flexural waves. Perhaps the amplitude resolution of the measurement system was not sufficient to resolve this difference.

Although it is most convenient to separate the longitudinal component by measuring the normal accelerations (because a single measurement at each point allows for the determination of both the longitudinal and flexural powers), it is not necessary to make the measurement in this way. Instead, the accelerometers can be oriented to measure the in-plane component of the acceleration directly. By making measurements on both sides of the beam, the in-plane motion due to the flexural vibration can be canceled out. This is the technique used in these measurements. The consequence is simply that the number of measurements is doubled, because of the need to make an in-plane and an out-of-plane measurement at each point and both sides of the structure must be accessable to the experimentalist, limiting somewhat of the usefulness of the approach in practical applications. When measuring out of plane accelerations, the longitudinal power flow component was also calculated, although the results were usually incorrect. At some instances, usually at the lower frequencies, the longitudinal power flow was correctly determined with this method.

This work has shown that for a beam-like structure with co-existing flexural and longitudinal vibration waves, the structure borne flexural and longitudinal powers can be calculated and measured. In accomplishing this, some interesting consequences of the effects of a junction on vibrations were observed.

When a longitudinal wave is traveling down a beam, and approaches a junction with another beam, it can excite flexural waves in the initial beam, as well as the intersecting beam. As has been shown, it can also excite a flexural wave in the initial beam which travels back towards the source of the longitudinal wave. Vibration source identification is commonly performed by looking at the phase relationship between two accelerometers which are oriented to measure the out-of-plane (flexural) acceleration, (as described in Bendat and Piersol (1986)). If this method of source identification on Leg A, at frequencies where the longitudinal wave excites a returning flexural wave, the flexural wave would be identified as traveling from the direction of the stem. While this is true, we know that the original source of that wave was the shaker, which is not in

the direction of the stem. Thus, misleading information about the origin of the vibration will result from using the phase method of source identification.

Another consequence of the observation that one wave type excites vibration of the other wave type is that conventional damping treatments can be surprisingly ineffective in reducing vibration or noise. Typical damping treatments are designed to damp flexural vibration. Two examples of these treatments are constrained (or free) layer damping, and tuned vibration absorbers. Both treatments are not very effective in reducing the power associated with longitudinal vibration. In a structure which consists of several attached members, it may not be sufficient to apply damping to only some parts of the structure. The remaining longitudinal waves will still be free to travel throughout the structure, and can excite flexural waves in other areas. Thus, the noise source will simply be shifted to another area. Vibration control treatments which reduce longitudinal waves, or joint designs which restrict the transmission of selected wavetypes may be required.

Although this was not a study of joints, the two cases that we had demonstrated that the power flow across the bolted joint (into the stem) is similar to the power flow for the continuous joint. The particular joint design for this test was probably a better joint than is found in practice, because of the well machined smooth and flow surfaces, and because steel bolts were used to join plastic parts. Less ideal joint designs may well transmit less power. The significance of these results however, is that for well machined joints, a bolted structure can act like a continuous one.

Finally, the good agreement between the measurement and the calculations serves as a validation of both efforts.

In the future, this work should be expanded so that the measurements can be made on one side of the beam only, and with a scanning laser vibrometer. Because of the bias errors introduced by the standing waves when measurements are not made at spacings of a quarter of a wavelength, it is necessary to make vibration measurements at different spacings in order to determine the power at different frequencies. If one is interested in a single frequency, this is not much of a problem, although it must be remembered that the quarter wave spacing is different for the flexural and longitudinal waves when setting up the experiment. If one is interested in a broad frequency range, and detailed power measurements are desired to produce a contour plot, it is best to make measurements at small spacings, and in the data analysis, merely use the data from the spacings that are appropriate for the frequency of interest. At higher frequencies, merely use the data from a more finely spaced collection of sensor outputs. While it is possible to obtain measurements at small spacings using a roaming accelerometer, this is tedious, and placement errors are invariably introduced. A scanning laser removes the tedium, and the control over the spacing between measurement points is presumably much more exact.

The necessity to make measurements at quarter wavelength spacings does not necessarily imply an apriori knowledge of the wavespeed of the material. As has been discussed earlier, the use of frequency response measurements instead of the more typical cross spectrum provides the data to obtain the mode shapes at any frequency of interest. Previously, it was mentioned that these mode shapes were examined merely to determine of the longitudinal vibration had been successfully extracted from the total vibration of the structure. The mode shape can certainly be looked at to determine the length of the quarter wavelength. In these measurements, data were obtained at spacings of 2 inches. When the quarter wavelength was identified, the data points which were spaced appropriately were used in the power calculations.

Three drawbacks to the use of a laser do exist. The signal to noise ratio will be less when measuring velocities, rather than accelerations. This will become more of a problem at the

higher frequencies. The second drawback with the laser is the current need to make measurements on both sides of the beam. This will require some thought to design a functional setup, perhaps involving mirrors to bend the laser beam to the opposite side. While the laser could simply be moved to the other side of the beam after the first side is scanned, it may be a challenge to insure that the measurement points on the second side are directly opposite the initial points. This is a surmountable challenge, however, and should not be used to disqualify the use of the laser. The third challenge originates in our measurements, which were not able to extract the longitudinal power with measurements normal to the surface. Because a single laser beam will measure the normal velocity only, the problems which were encountered with the normal accelerometer measurements must be fully understood.

- Conclusions

This work has demonstrated that:

- techniques exist for measuring structural vibration power flow due to flexural and longitudinal vibrations, even when they coexist on a beam;

- longitudinal waves can act as a source which excites flexural waves in a structure and flexural waves can act as a source which excites longitudinal waves in a structure. Although it has been known from theoretical considerations that this must occur, this work is the first known experiment to demonstrate this phenomena. One consequence of this interaction is that typical source identification measurements which consider only flexural components can be mislead into mis-identifying the source of a vibration problem. Another consequence is that vibration control treatments such as constrained (or free) layer damping may have limited effectiveness when longitudinal waves carry power. This is especially likely in structures which have coupled members;

- When a travelling wave encounters a junction, it takes the path of least resistance. It travels most efficiently into which ever receiving branch is at resonance, regardless of the type of vibration that is associated with the resonance;

- Finite Element techniques do successfully determine the structural vibration power flow due to flexural and longitudinal vibrations, even when they coexist on a beam;

- for two beams which intersect at right angles with a well mated surfaces and tight bolts, the general trends and levels of the longitudinal wave and flexural wave power flow across the intersection are the same, regardless of whether the intersection is continuous, or bolted. For the two joints considered in this test, the bolted joint passes an equivalent amount of power across the joint as the continuous beam did. This suggests that a bolted structure can be a good structural representative of a continuous structure.

Both experimental and finite element methods have been shown in this study to produce accurate longitudinal and flexural power flow fields in beam structures. Attempting to diagnose structure-borne noise problems using only a single approach however, would not be wise. Both techniques have strengths and weaknesses. Fortunately, the strengths and weaknesses of the two methods are complementary:

Strength: Finite element methods compute easily structure-borne power fields due to all wavetypes everywhere in a model.

Weakness: Experimental methods cannot, as yet, measure structure-borne powers carried by all wavetypes, and are sometimes difficult and time consuming to apply at all locations in a structure.

Weakness: Finite element models of complex structures are sometimes hard to develop, due to uncertainties regarding material properties and boundary conditions.

Strength: Experimental methods are insensitive to uncertainties regarding material properties and boundary conditions since they are applied to the actual structure.

Collaborative efforts using both experimental and finite element approaches are needed to diagnose successfully structure-borne noise problems. Experimental methods can be used to help develop finite element models by providing modal analysis, accelerance spectra, and first order power flow data, against which the response of the finite element model can be compared. Once a valid model is developed, it can be analyzed easily using McPOW to give a complete representation of the power flow field in the structure. The structure-borne power field could then be examined to identify dominant power flow paths. Also, areas on the structure where flexural waves transmit high levels of power could be targeted for effective vibration damping treatments. The effectiveness of damping the flexural waves can be examined in light of the ratio of the flexural wave power to the power in the other wavetypes. Candidate treatment designs could be tested using the validated finite element model prior to physically implementing them.

Acknowledgments:

The guidance of Drs. Burroughs and McDevitt at Pennsylvania State University in developing the measurement techniques are gratefully acknowledged.

The constant support of Dr Frank Peterson of the Naval Surface Warfare Center, and Dr. Peter Majumdar, of the Office of Naval Research are especially recognized, and appreciated.

APPENDIX A - Derivation of Power Flow expressions for Longitudinal Waves

Instantaneous power is the product of the component of the force which is in-phase with the velocity; or:

$$J(x,t) = F \cdot v \tag{A1}$$

Since Force, F can be written as $F = -SE\frac{\partial \varsigma}{\partial x}$, (using the convention that a tensile force is negative) the instantaneous power can be expressed as

$$J(x,t) = -ES\frac{\partial \varsigma}{\partial x}\frac{\partial \varsigma}{\partial t}. \tag{A2}$$

The spatial derivative of the in-plane displacement can be determined using the finite difference approximation:

$$\frac{\partial \varsigma}{\partial x} = \frac{1}{\Delta}(\varsigma_2 - \varsigma_1) \tag{A3}$$

and the time derivative of the in-plane displacement can be determined from:

$$\frac{\partial \varsigma}{\partial t} = \frac{j\omega}{2}(\varsigma_1 + \varsigma_2). \tag{A4}$$

Combining equations A2, A3, and A4, , and using accelerations instead of displacements, where for time harmonic waves $\ddot{\varsigma} = -\omega^2\varsigma$, the instantaneous power is determined from:

$$J(x,t) = \frac{jES}{2\Delta\omega^3}(\ddot{\varsigma}_2 - \ddot{\varsigma}_1)(\ddot{\varsigma}_2 + \ddot{\varsigma}_1). \tag{A5}$$

The time averaged power is usually of more interest than the instantaneous power, and can be obtained by noting that for two time varying quantities, a(t) and b(t), their time averaged product is

$$\langle a(t)b(t)\rangle_t = \frac{1}{T}\int_{-\infty}^{\infty} a(\omega)b^*(\omega)d\omega \tag{A6}$$

which reduces to $\frac{1}{2}\left(a(\omega)\cdot b^*(\omega)\right)$ for a single frequency. This quantity can be determined from a cross spectral density, as $G_{ba}/2$. Therefore, the time averaged longitudinal power is

$$J(x,f) = \frac{jES}{2\Delta\omega^3}\left[G_{\ddot{\varsigma}_2\ddot{\varsigma}_2} + G_{\ddot{\varsigma}_2\ddot{\varsigma}_1} - G_{\ddot{\varsigma}_1\ddot{\varsigma}_2} - G_{\ddot{\varsigma}_1\ddot{\varsigma}_1}\right] \tag{A7}$$

Using the relationship that $G_{21} = G_{12}^*$, and noting that the cross spectral densities are complex, and that the imaginary part of an auto spectral density =0, one can show after some algebra that the active power, which is the real part of J(x,f), is:

$$J(x,f) = -\frac{ES}{\Delta\omega^3}\Im\{G_{\varsigma_2\varsigma_1}\} \tag{A8}$$

and 1/2 of this amount for a single frequency.

The above expression employs the cross spectral density of the in-plane acceleration. Baker (1989) takes this expression one further step, by allowing the use of the cross spectral density of the normal accelerations with:

$$J(x,f) = -\frac{ESv^2}{\Delta\omega^3}\Im\{G_{\xi_2\xi_1}\} \tag{A9}$$

APPENDIX B - Theoretical Decay of Power in Bending Waves

The amplitude of a damped harmonic oscillator decays as $Ae^{-\beta t}$, according to Kinsler and Frey (1982). Examining the exponent, β is a decay constant, which equals

$$\beta = \frac{\omega_o \eta}{2}$$

The time can be expressed as $\frac{x}{v_B}$.

Therefore:

$$\beta t = \frac{\omega_o \eta t}{2} = \frac{\omega_o \eta x}{2 v_B} = \frac{\omega_o \eta x}{2\sqrt{\omega c \kappa}} = \sqrt{\frac{\omega}{c\kappa}} \frac{\eta x}{2}$$

since $v_B = \sqrt{\omega c \kappa}$.

Because the flexural wave number $k_B = \sqrt[4]{\frac{\rho S \omega^2}{EI}}$,the longitudinal phase speed $c = \sqrt{\frac{E}{\rho}}$,the radius of gyration $\kappa = \frac{h}{\sqrt{12}}$ and the momemt of Inertia $I = \frac{1}{12} b h^3$, then

$I = bh\kappa^2 = S\kappa^2$

and finally, $k_B^4 = \frac{\omega^2}{c^2 \kappa^2}$.

Consequently, $\beta t = \frac{k_B \eta x}{2}$ and $e^{-\beta t} = e^{-\frac{k_B \eta x}{2}}$.

As an example, one can calculate the reduction in amplitude from the drive point (x=0) to a point 50 inches away. At 500 Hz, the bending wave number is 15.2 m^{-1} . Assuming a loss factor of 0.007, then $e^{-\frac{k_B \eta x}{2}} = 0.9346$, so that the amplitude is expected to reduce to 93.46% of its value at the drive point when the wave has traveled a distance of 50 inches.

REFERENCES

Baker et.al.;"Laser Technology for Measuring Vibrational Power Transmission in Beam Like Structures", Proceedings of Third International Conference on Stress Analysis by Thermoelastic Techniques: Recent Developments in Industrial Measurement and Analysis; 14-16 March 1989, London England, 160-170.

Bendat and Piersol,"Random Data"; Wiley and Sons, 1986.

Carroll; "Structural Response and Power Flow Measurements Utilizing Cross Spectra"; Ph.D. Dissertation, Catholic University of America, Washington DC, 1987.

Cremer, Heckl, and Ungar, "Structure Borne Sound", Springer-Verlag Press, 1966.

Fahy; "Measurement of Mechanical Input Power to a Structure"; Journal of Sound and Vibration (1969) 10(3), 517-518.

Fahy and Pierri; "Application of Cross-Spectral Density to a Measurement of Vibration Power Flow between Connected Plates"; Journal of the Acoustical Society of America; vol 62, No 5, Nov 77.

Hambric, S.A., 1990, ``Power Flow and Mechanical Intensity Calculations in Structural Finite Element Analysis," ASME Journal of Vibration and Acoustics, Vol. 112, No. 4, pp. 542-549, 1990.

Hambric, S.A., "Influence of Different Wave Motion Types on Finite Element Power Calculations," Third International Congress on Intensity Techniques, Senlis, France, pp. 215-223, August 1990.

Hambric, S.A.; "Comparison of Finite Element Predictions and Experimental Measurements of Structure-Borne Powers in a T-Shaped Beam" Proceedings of Internoise 95, July 1995, 685-688.

Hambric, S.A., and Taylor, P.D., ``Comparison of Experimental and Finite Element Structure-Borne Flexural Power Measurements for a Straight Beam," Journal of Sound and Vibration, Vol. 170, No. 5, pp. 595-605, March, 1994.

Horner and White; "Techniques for Measuring Vibrational Power Transmission in a Beam-Like Structure Carrying Two Types of Wave"; Proceedings of International Congress on Intensity Techniques; Senlis France, 27-29 April, 1990, 273-280.

Kinsler, Frey, Coppens, Sanders, "Fundamentals of Acoustics"; Wiley and Sons, Third Edition, 1982.

Linjama and Lahti; "Estimation of Bending Wave Intensity in Beams using the Frequency Response Technique"; Journal of Sound and Vibration (1992) 153(1), 21-36.

McDevitt et.al; "Two Channel Laser Vibrometer Techniques for Vibrational Intensity Measurements Part 1: Flexural Intensity"; Transactions of the ASME Vol 115, October 1993, 436-440.

McDevitt et.al; "Two Channel Laser Vibrometer Techniques for Vibrational Intensity Measurements Part 1: Longitudinal Intensity"; Transactions of the ASME Vol 116, January 1994, 100-104.

NASTRAN User's Manual, NASA SP-222(08), Computer Software Management and Information Center (COSMIC), University of Georgia, Athens, Georgia, 1986.

Noiseux; "Measurement of Power Flow in Uniform Beams and Plates"; Journal of the Acoustical Society of America; vol 47, no.1 (part 2), 1970, 238-247.

Pavic; "Measurement of Structure Borne Wave Intensity, Part 1: Formulation of the Methods"; Journal of Sound and Vibration (1976) 49(2), 221-230.

Timoshenko & Goodier; "Theory of Elasticity", McGraw-Hill Book Co, 1951.

Verheij; "Cross Spectral Density Methods for Measuring Structure Borne Power Flow on Beams and Pipes"; Journal of Sound and Vibration; (1980) 70(1), 133-139.

THIS PAGE INTENTIONALLY LEFT BLANK

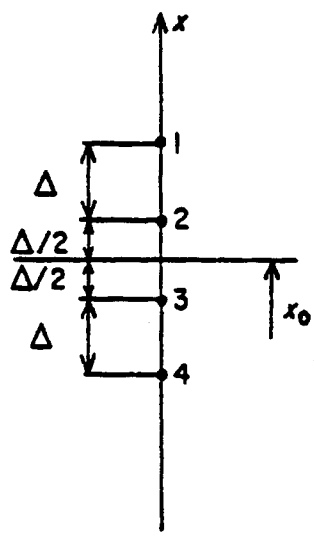

Figure 1. Orientation and numbering of transducer array.

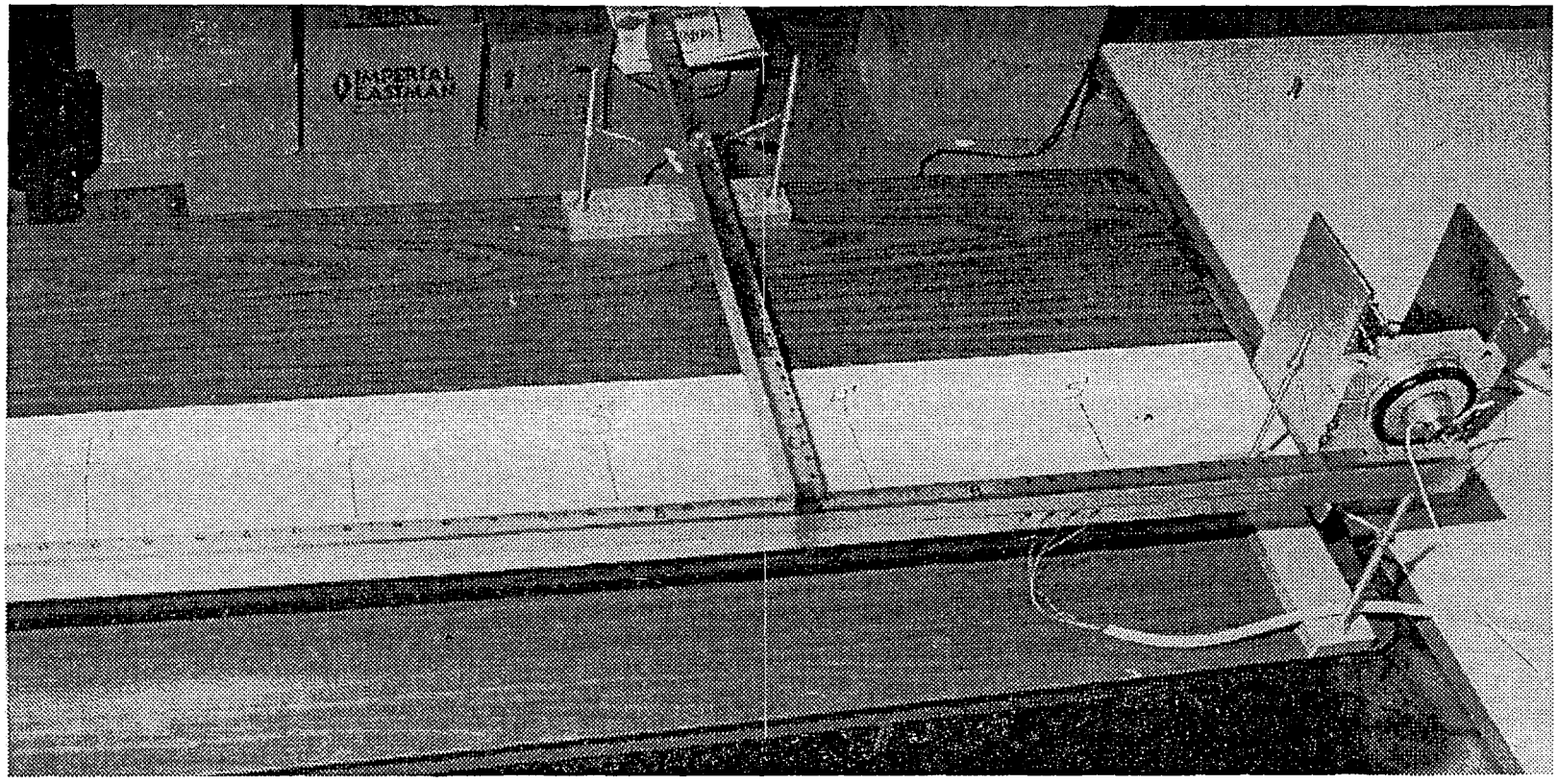

Figure 2. Photograph of T-beam.

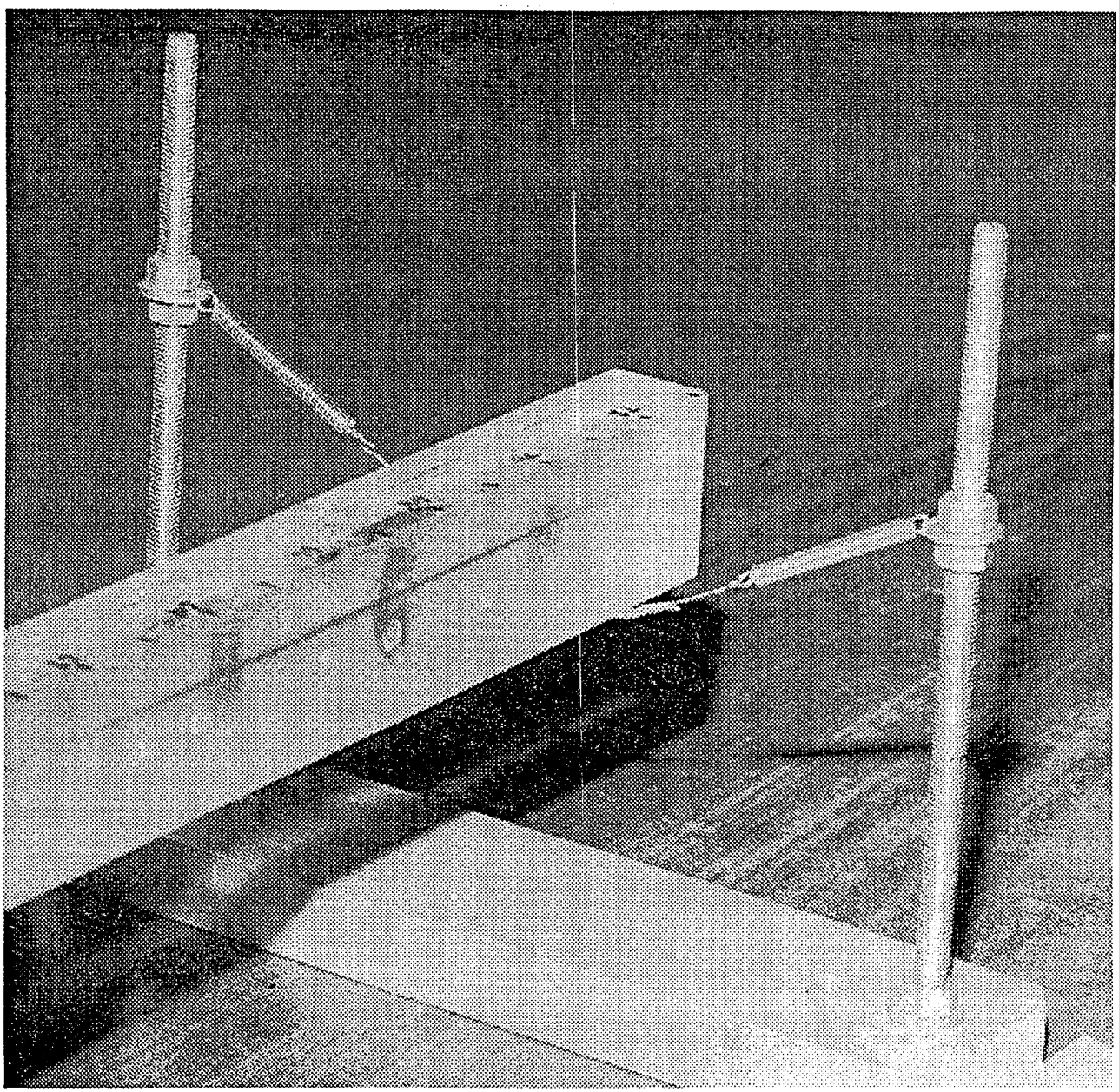

Figure 3. Photograph of support bridges.

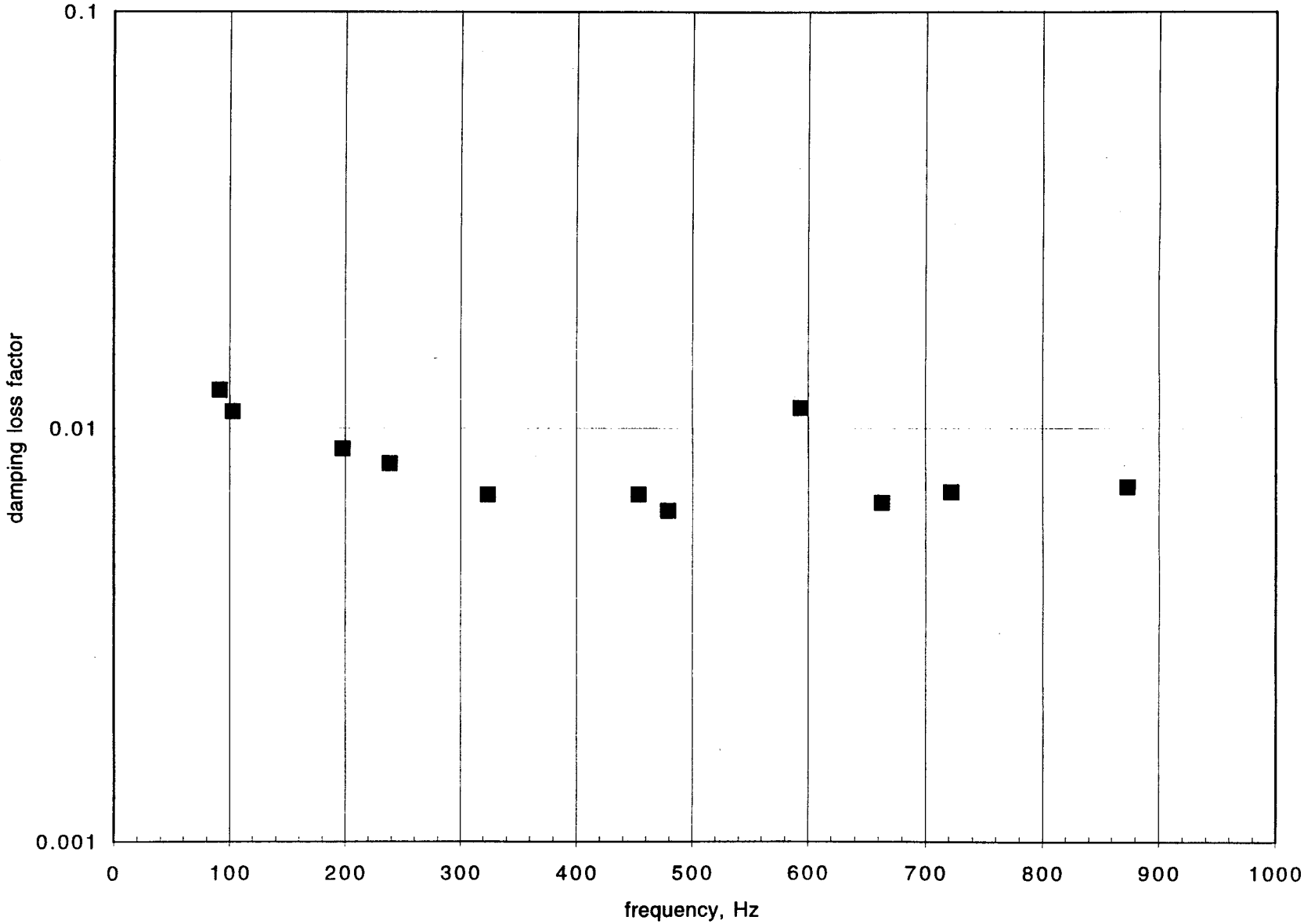

Figure 4. Measured damping loss factors of beam material.

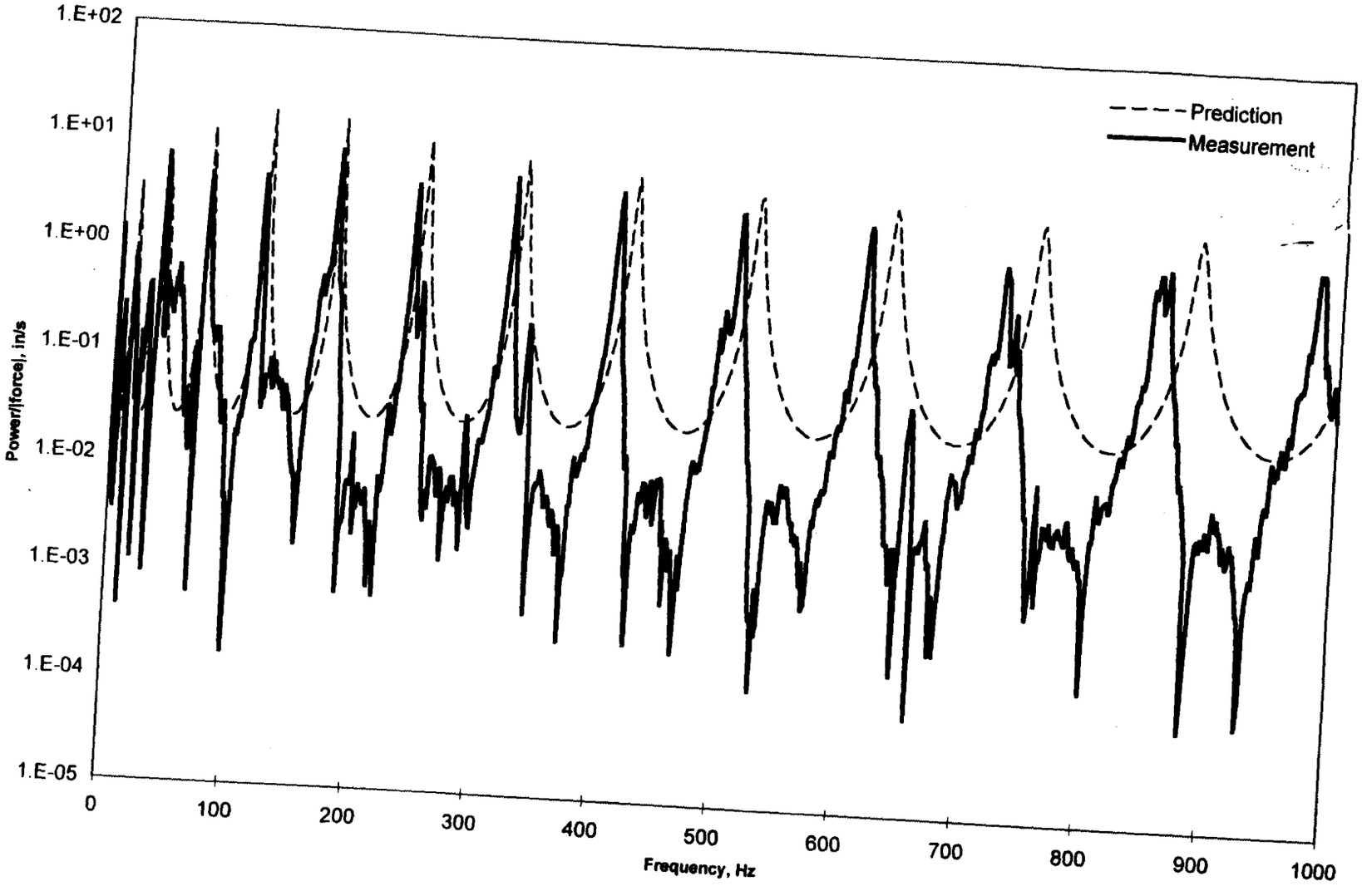

Figure 5. Flexural structure-borne input powers on straight beam.

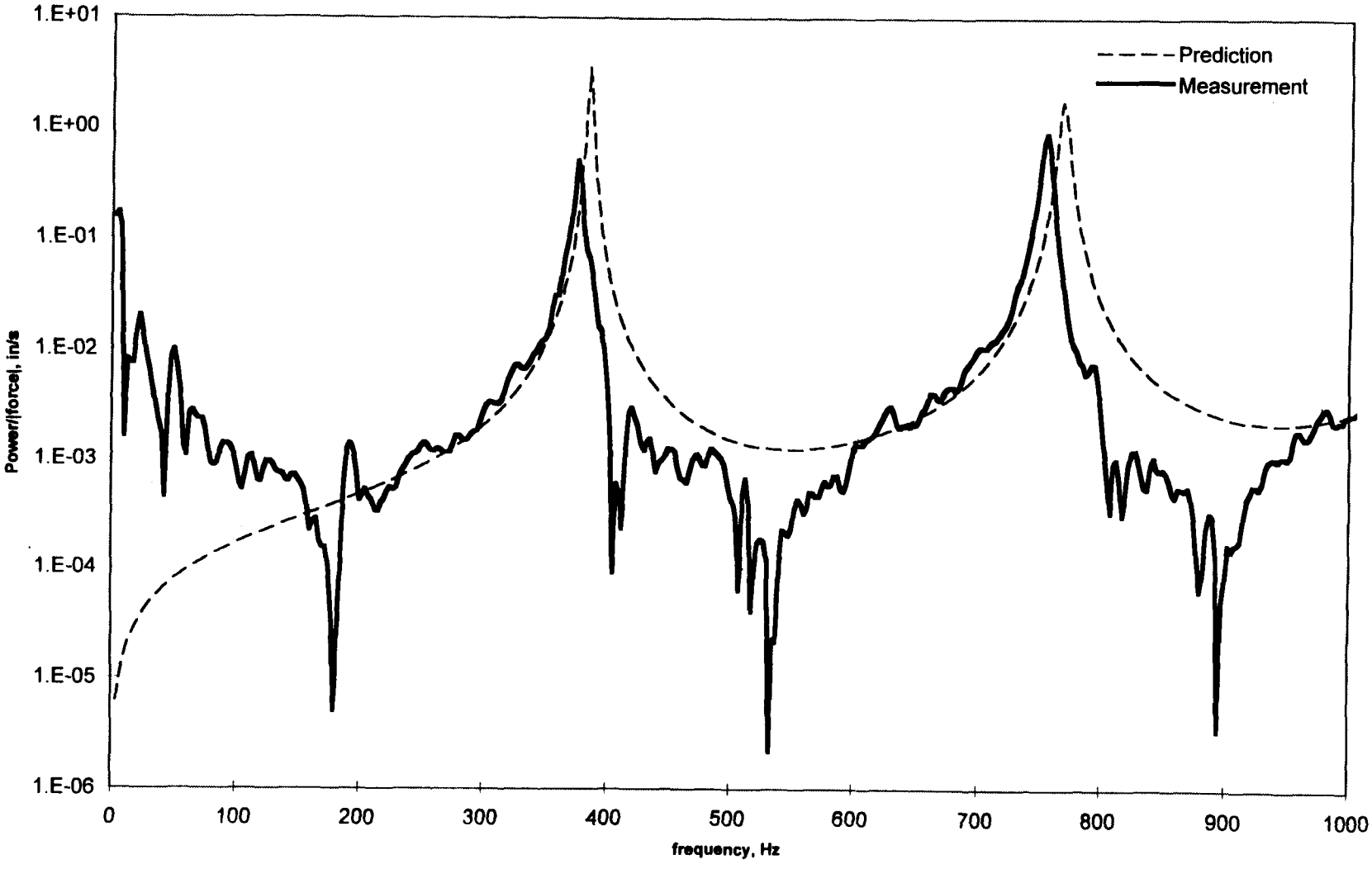

Figure 6. Longitudinal structure-borne input powers on straight beam.

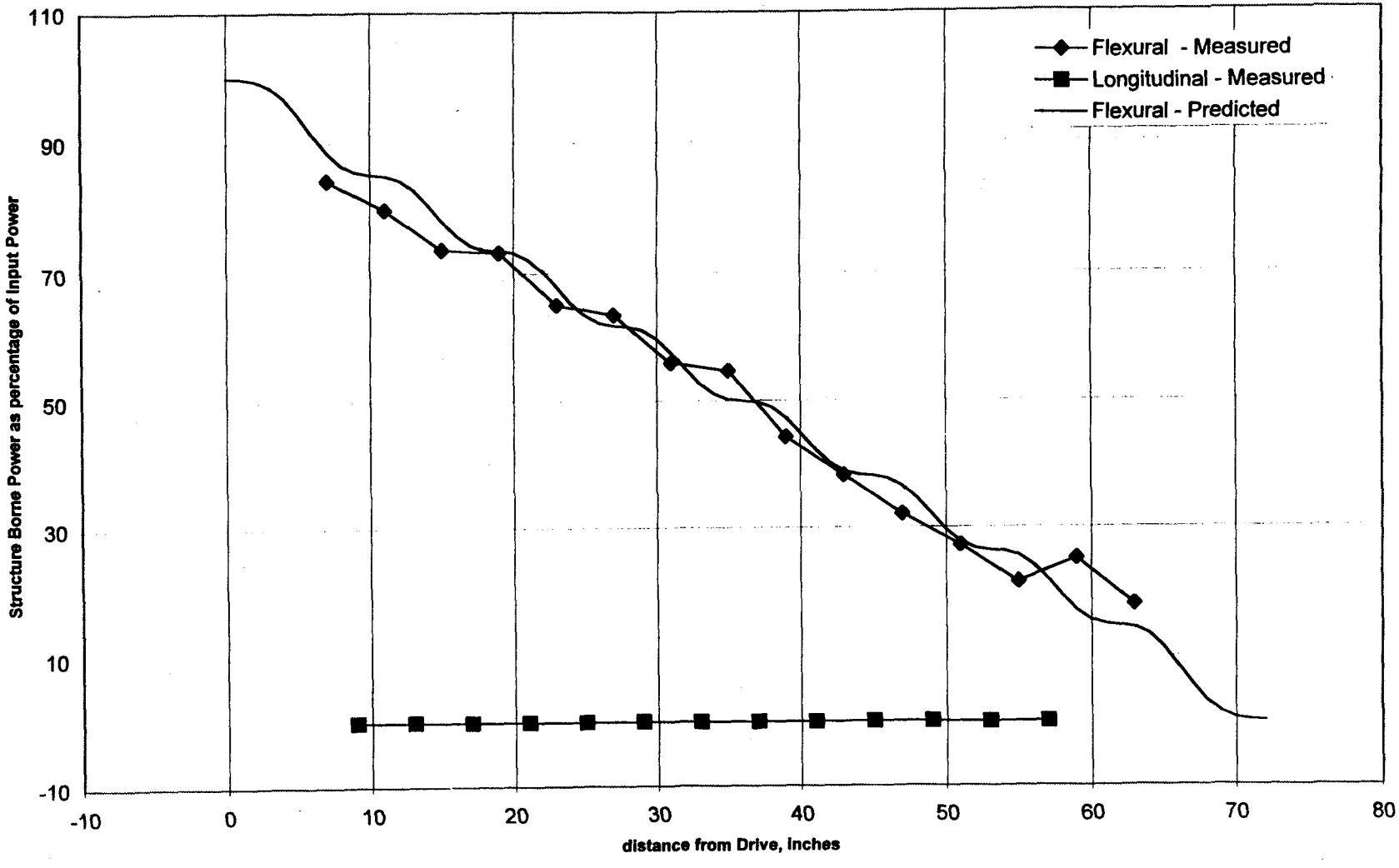

Figure 7. Flexural and longitudinal structure-borne powers on straight beam at 420 Hz.

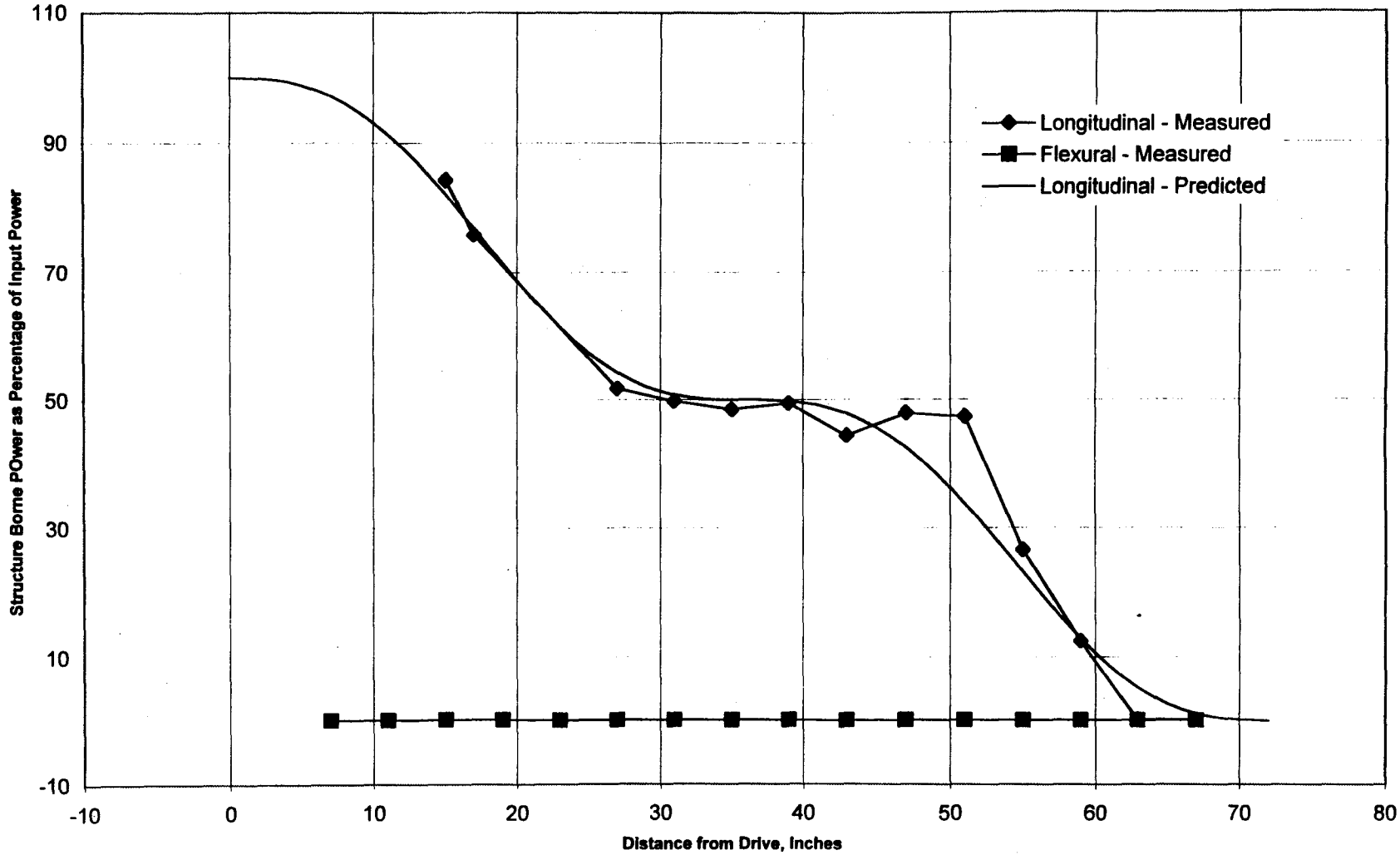

Figure 8. Flexural and longitudinal structure-borne powers on straight beam at 780 Hz.

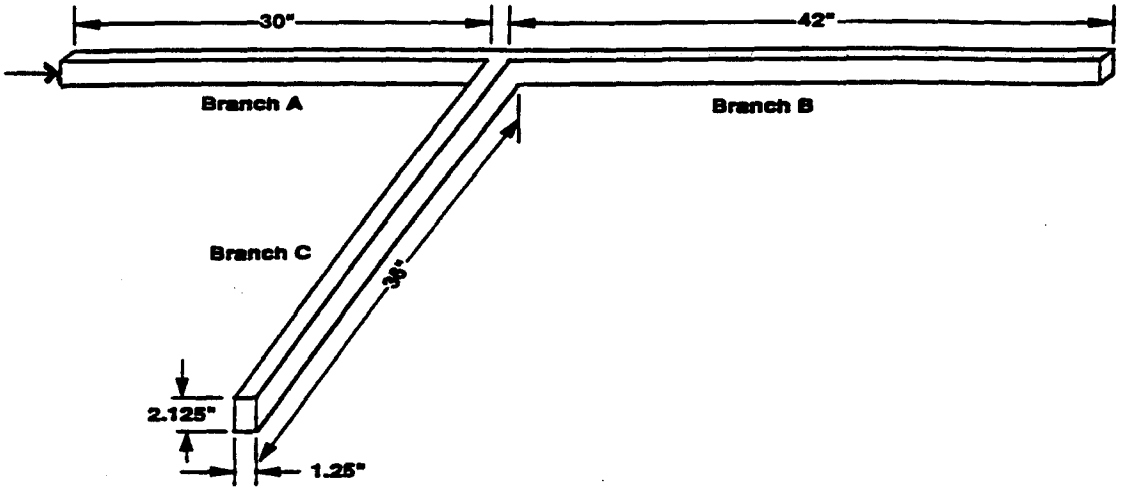

Figure 9a. Sketch of T-beam with axial force applied.

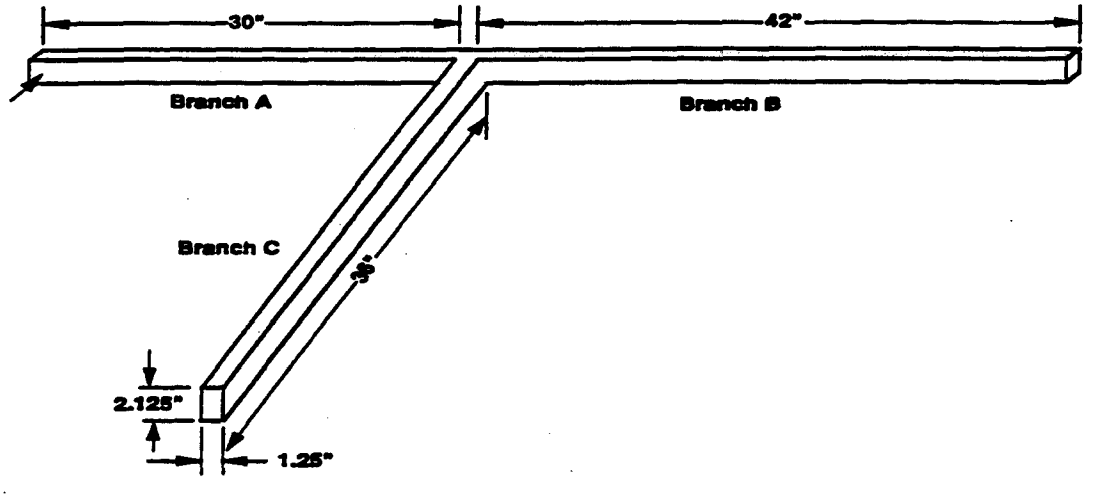

Figure 9b. Sketch of T-beam with longitudinal force applied.

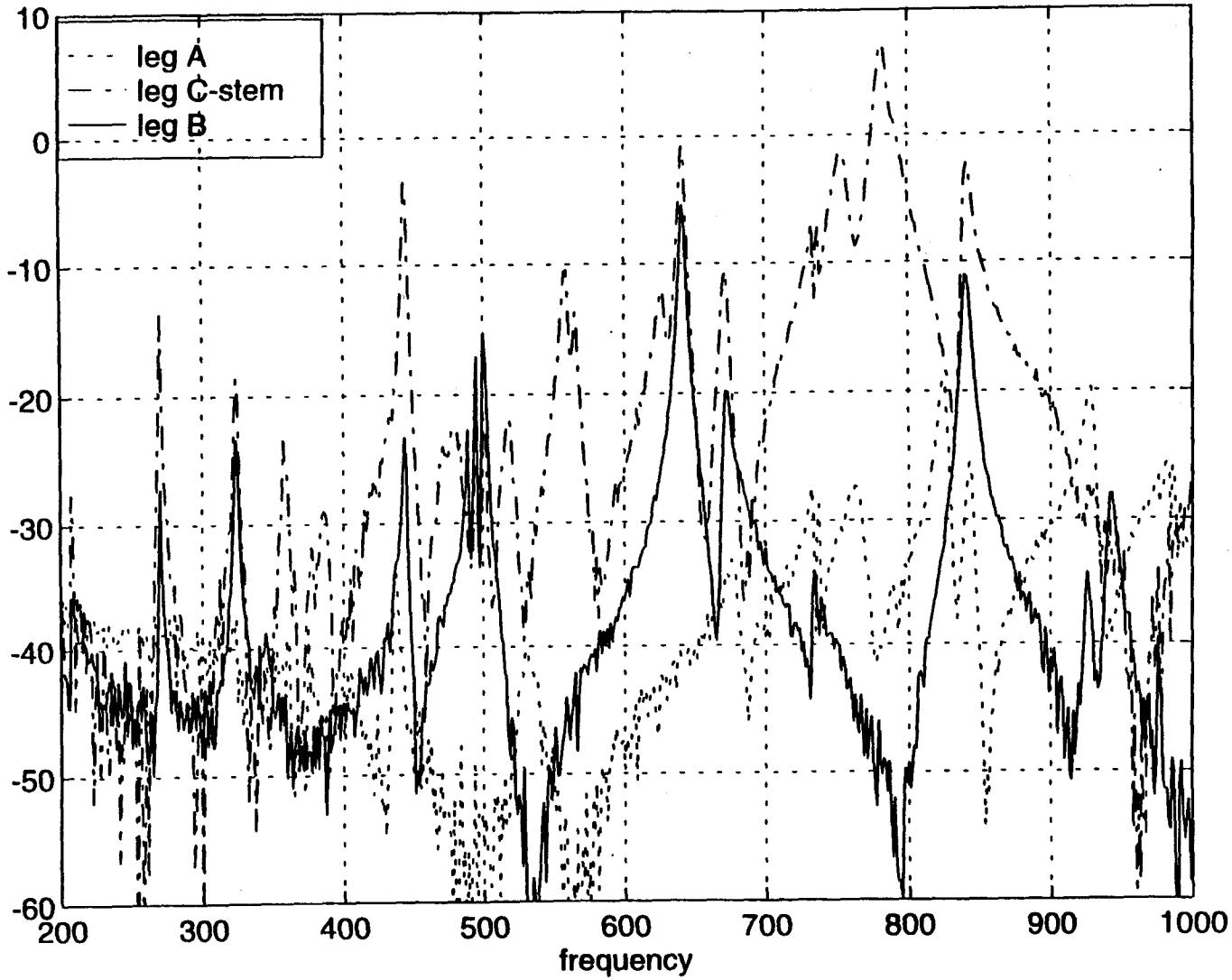

Figure 10a. Flexural resonances of T-beam branches.

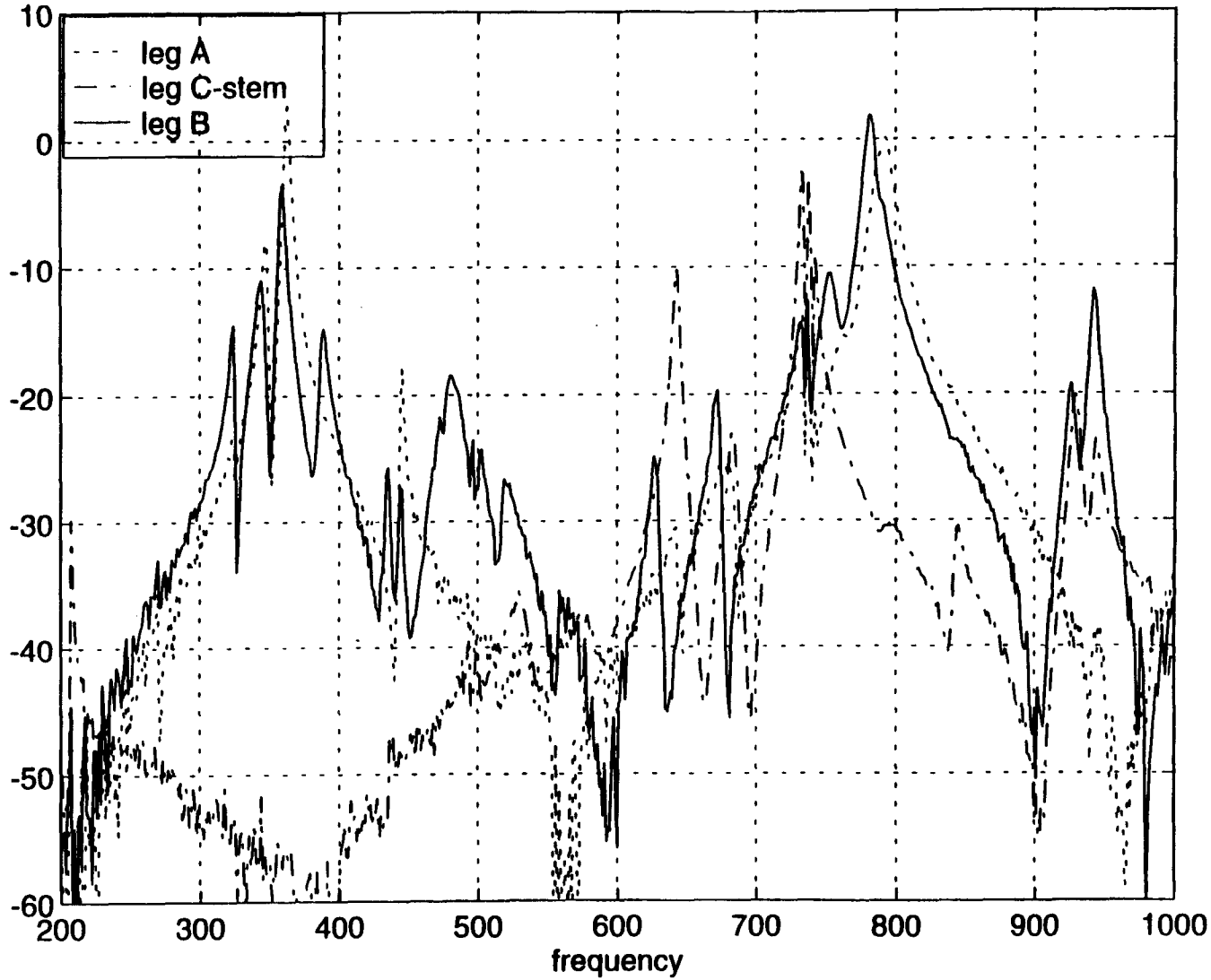

Figure 10b. Longitudinal resonances of T-beam branches.

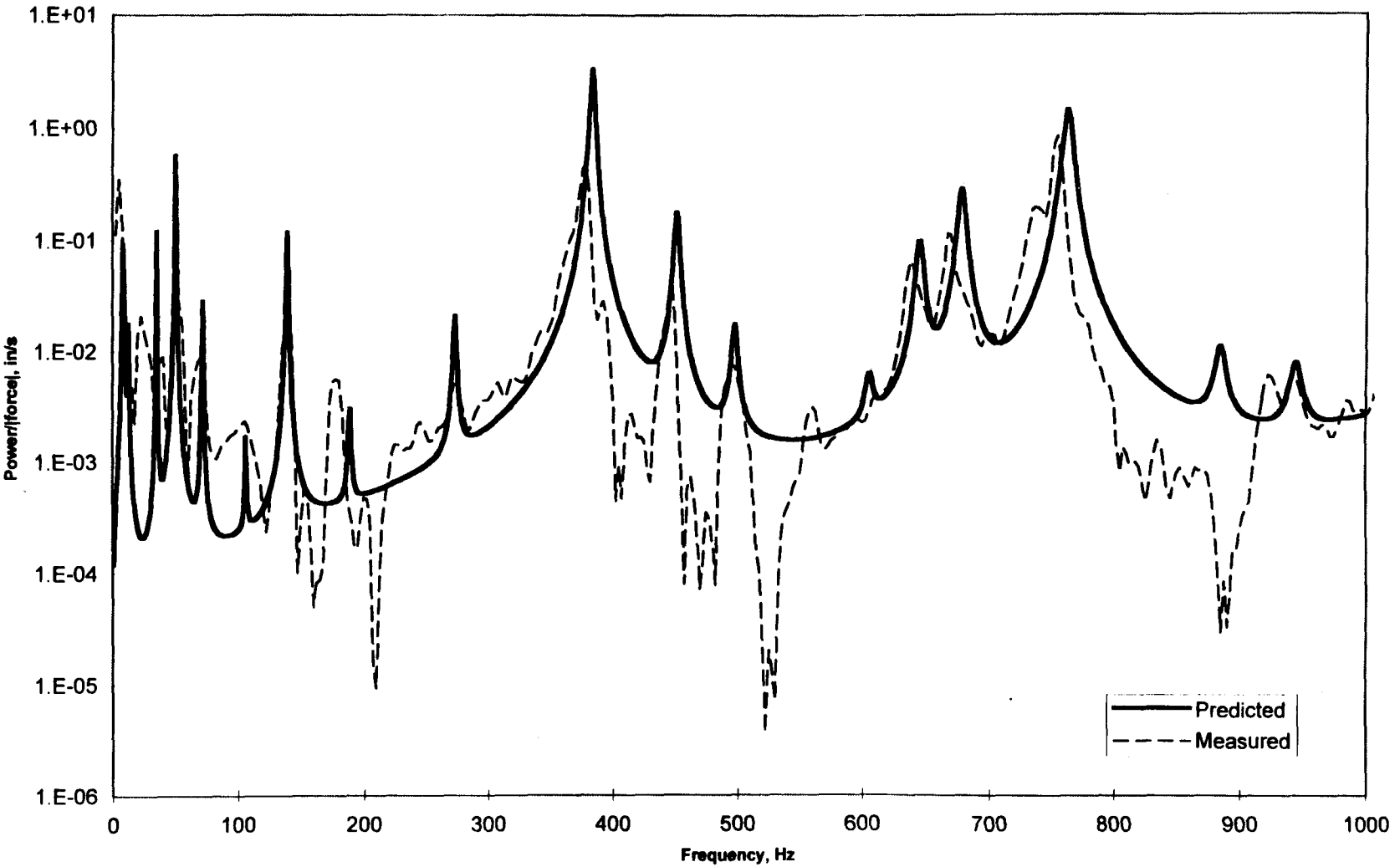

Figure 11. Axially power input to continuous T-beam.

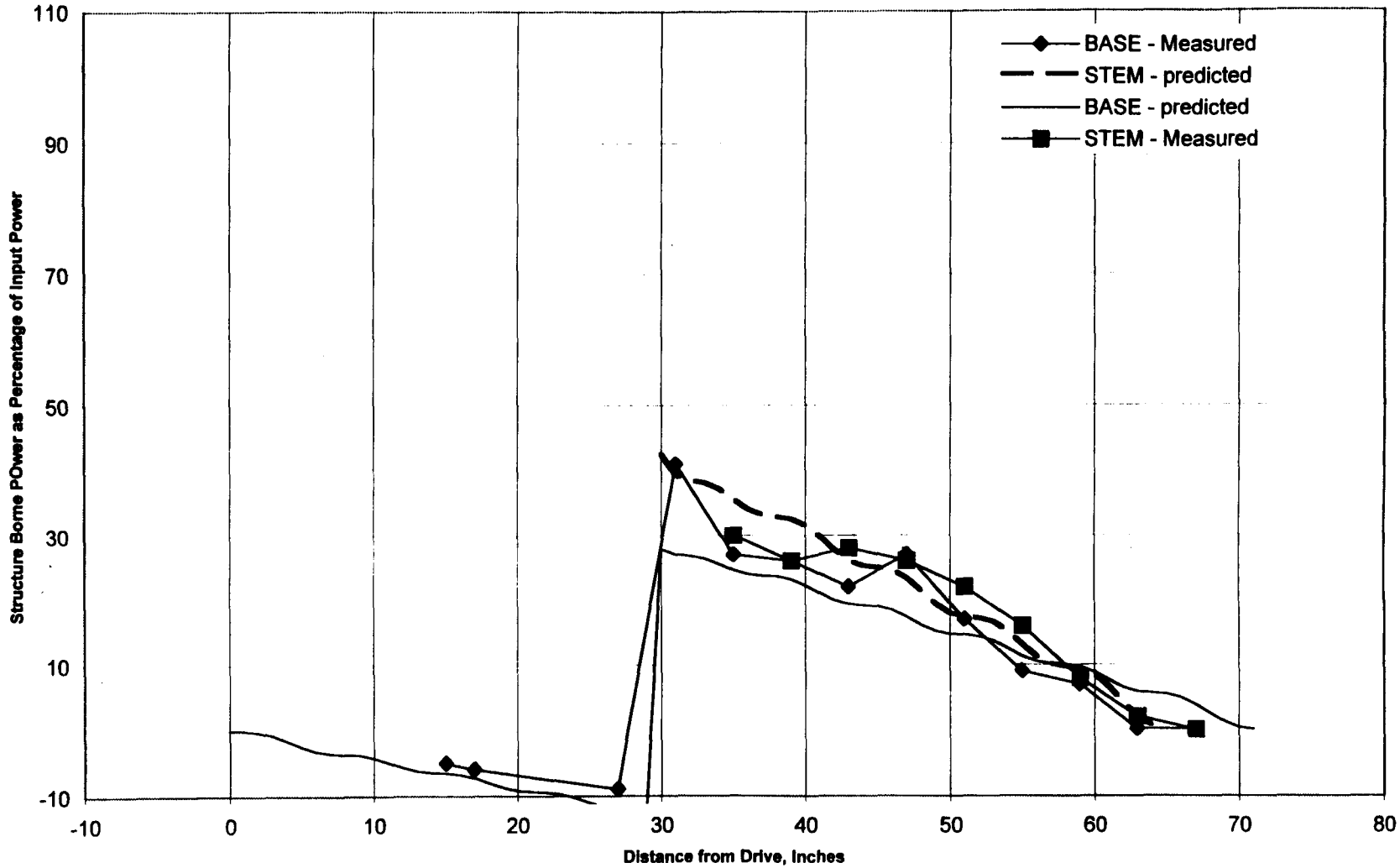

Figure 12. Flexural structure-borne powers on continuous T-beam at 670 Hz.

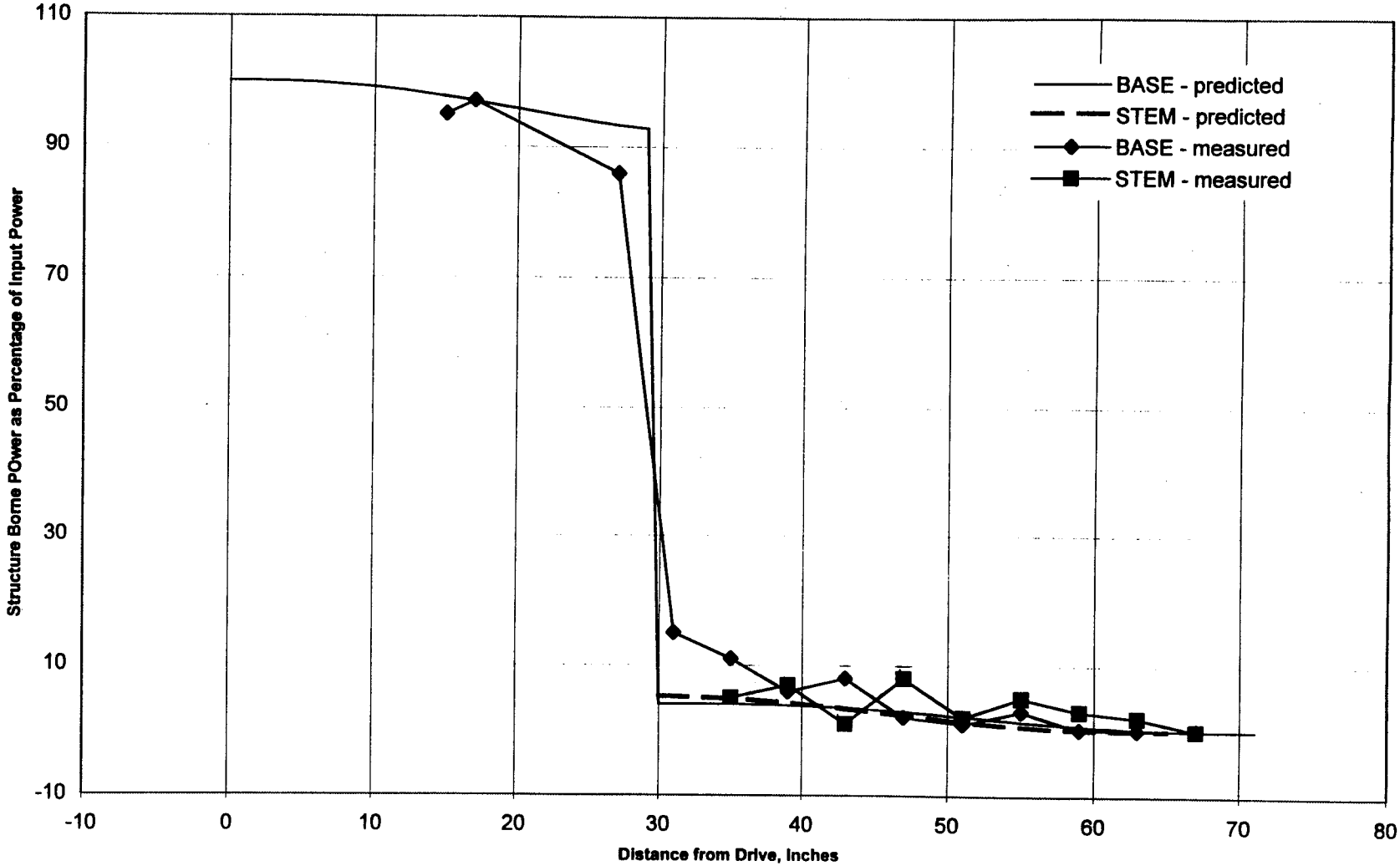

Figure 13. Longitudinal structure-borne powers on continuous T-beam at 670 Hz.

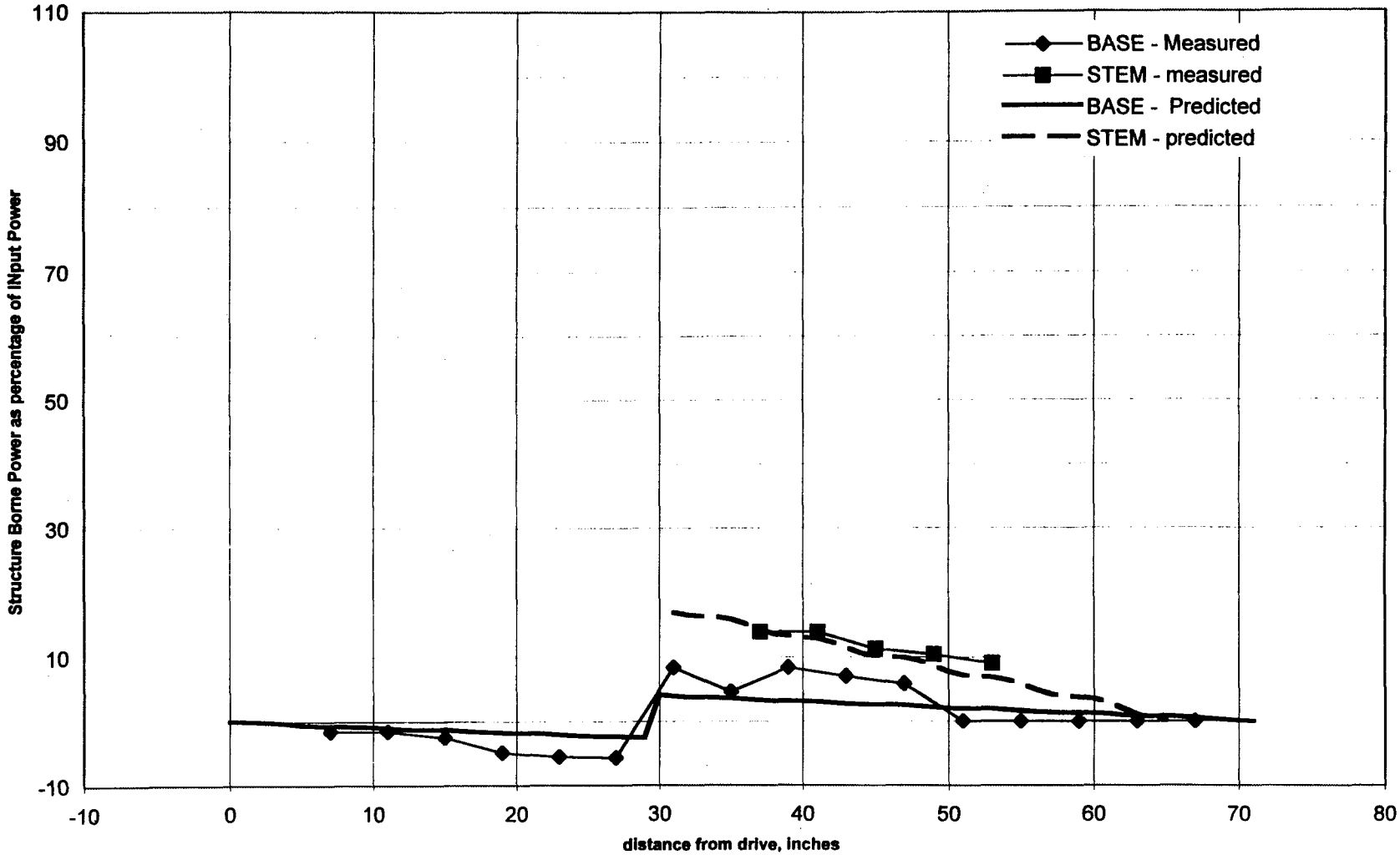

Figure 14. Flexural structure-borne powers on continuous T-beam at 735 Hz.

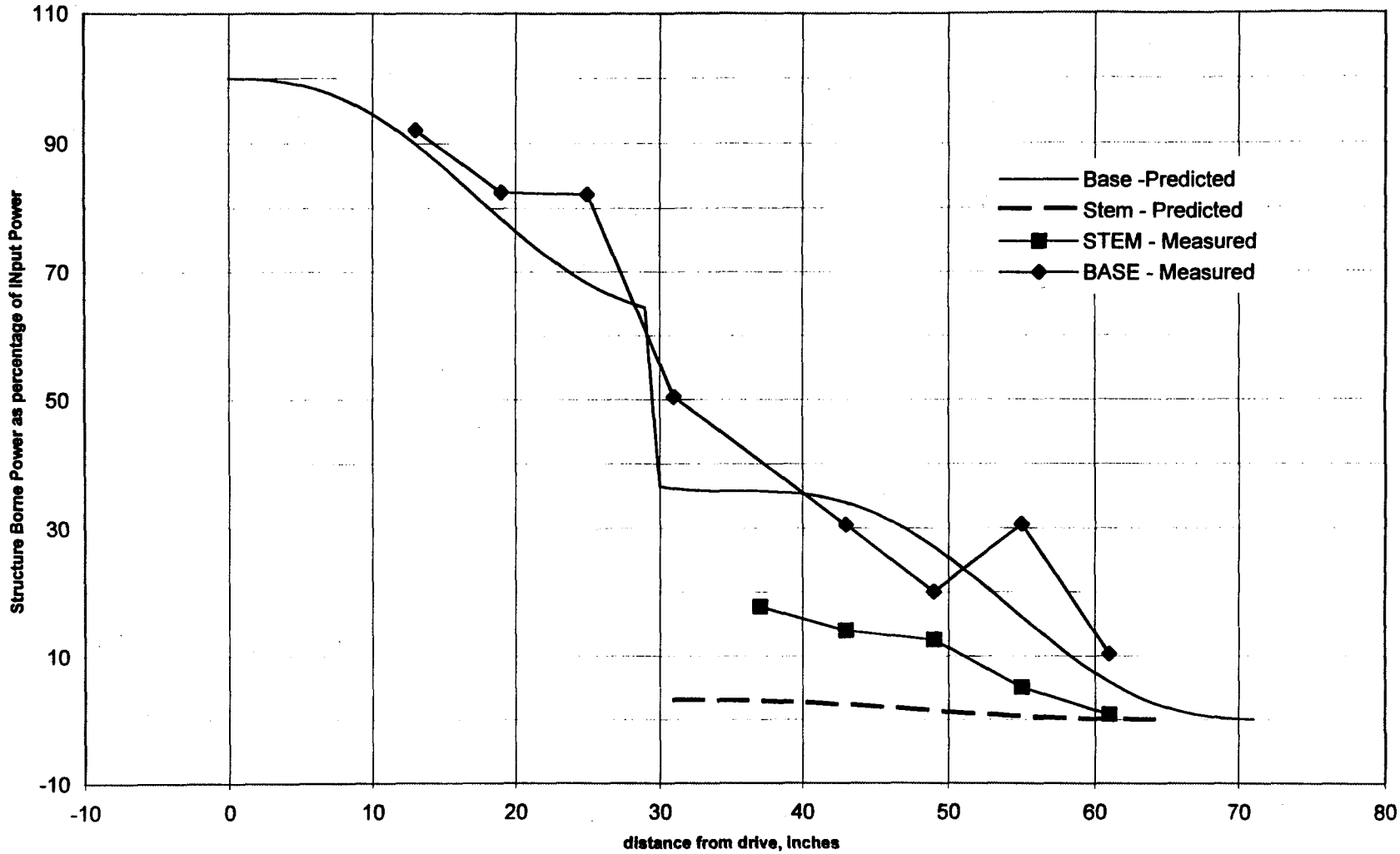

Figure 15. Longitudinal structure-borne powers on continuous T-beam at 735 Hz.

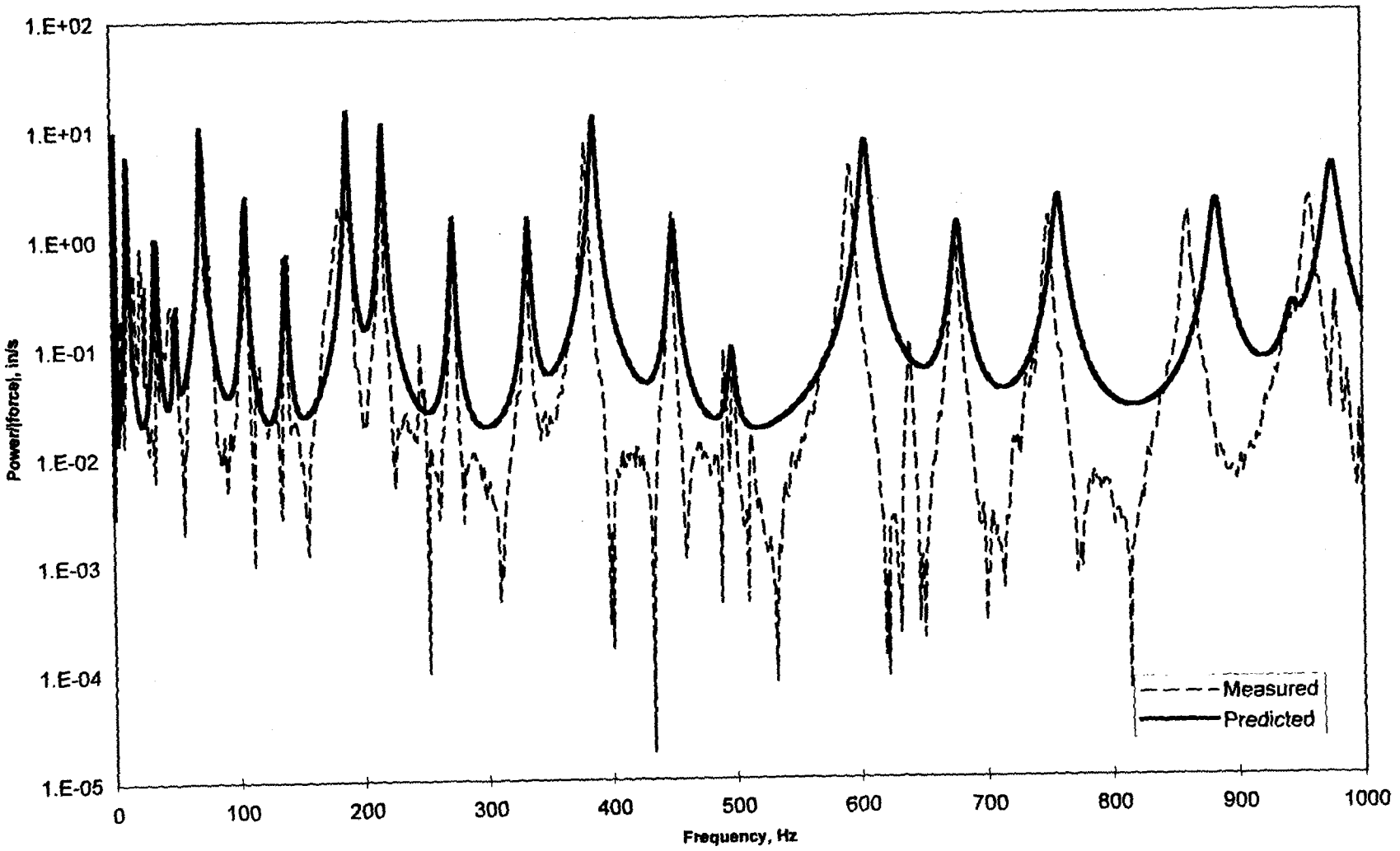

Figure 16. Flexural input power to continuous T-beam.

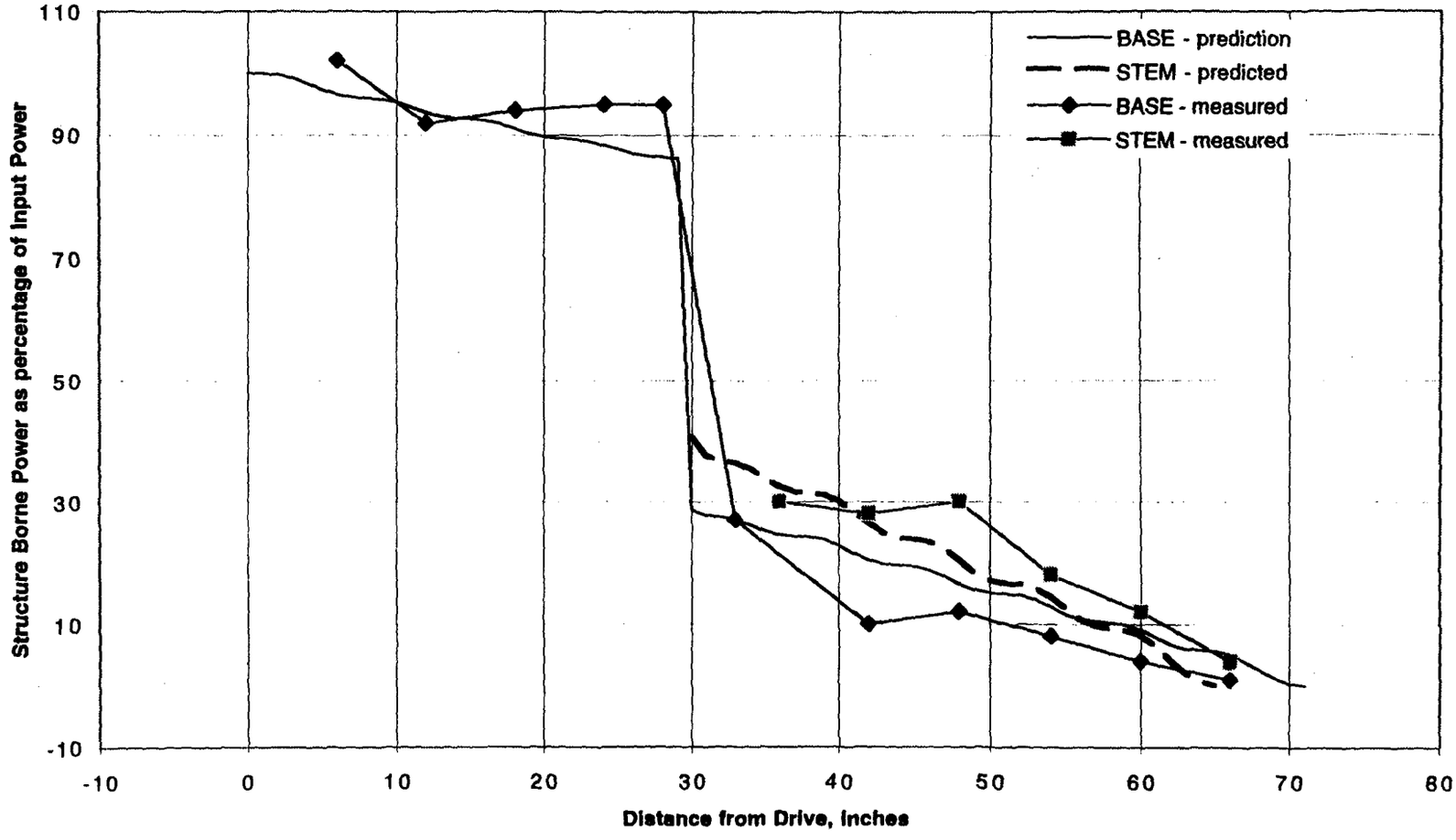

Figure 17. Flexural structure-borne powers on continuous T-beam at 670 Hz.

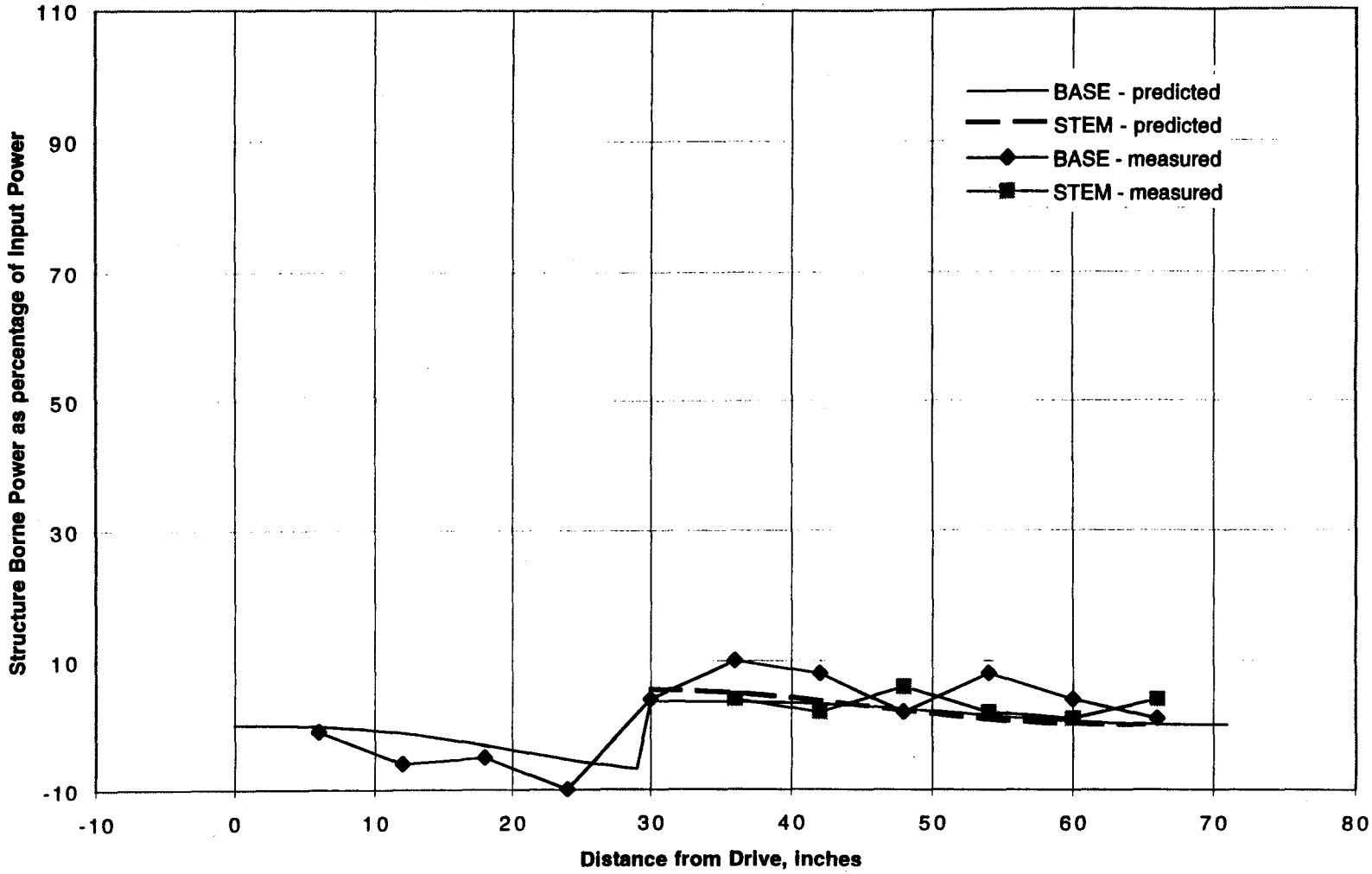

Figure 18. Longitudinal structure-borne powers on continuous T-beam at 670 Hz.

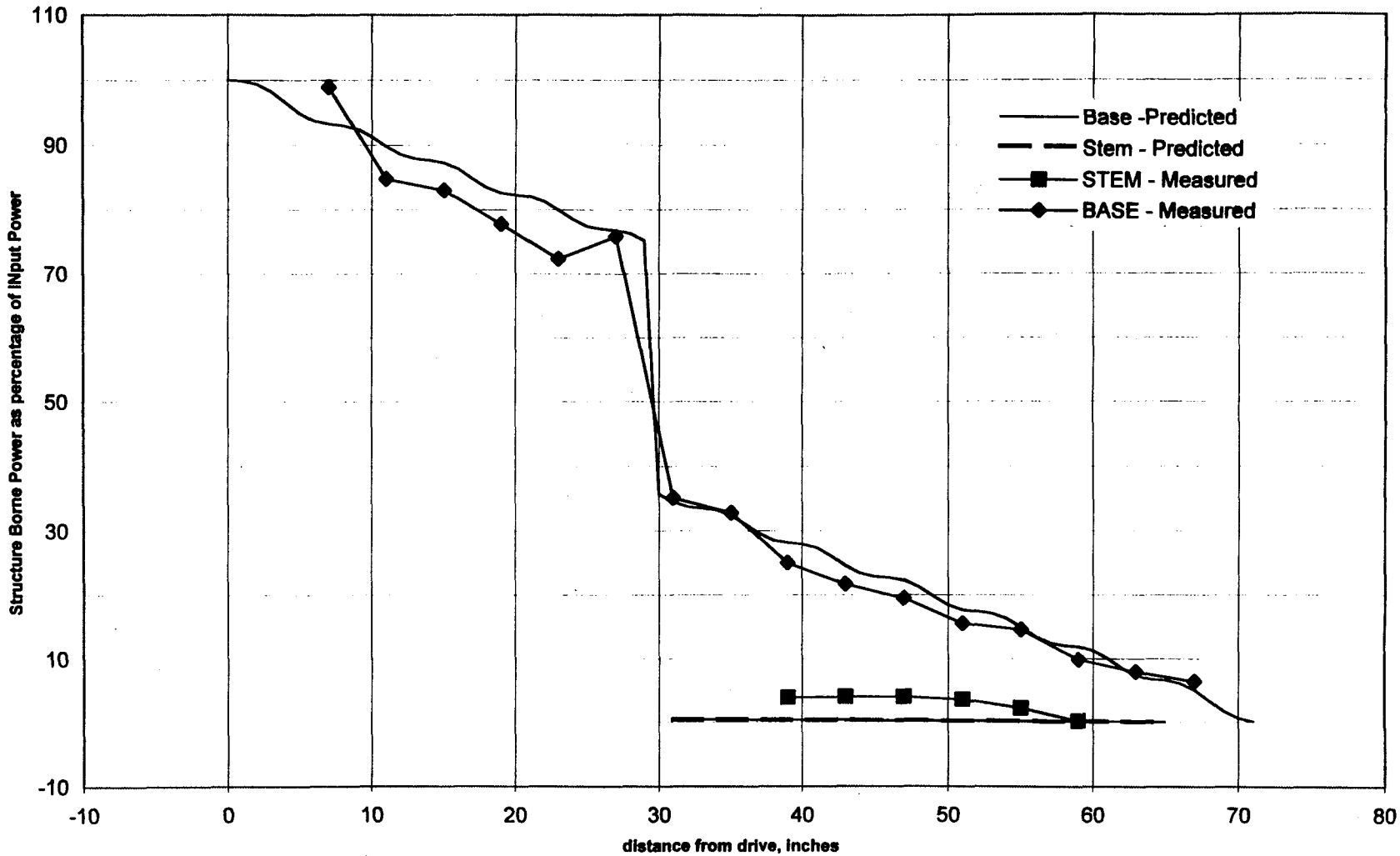

Figure 19. Flexural structure-borne powers on continuous T-beam at 735 Hz.

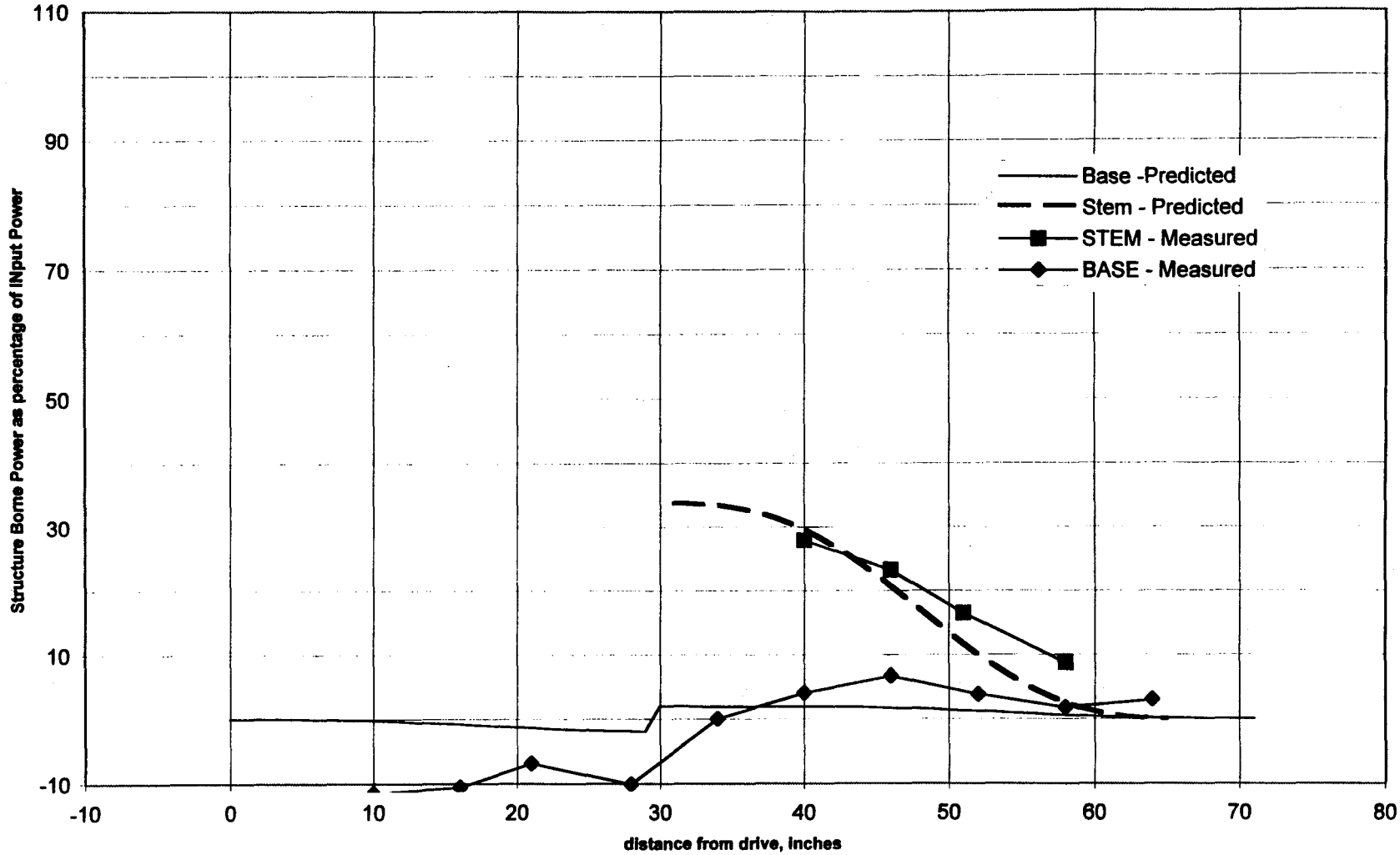

Figure 20. Longitudinal structure-borne powers on continuous T-beam at 735 Hz.

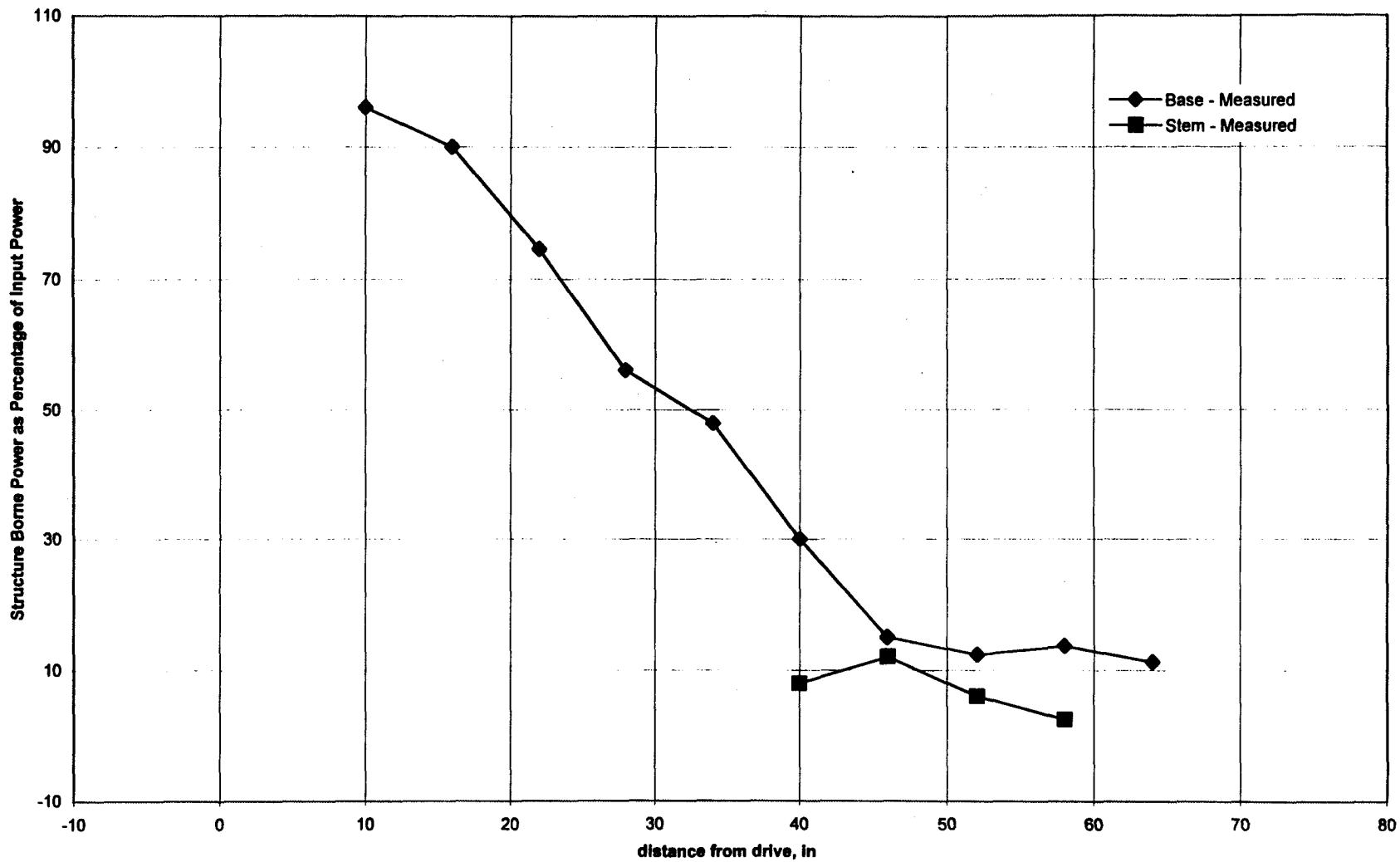

Figure 21. Flexural Longitudinal structure-borne powers on bolted T-beam at 735 Hz.

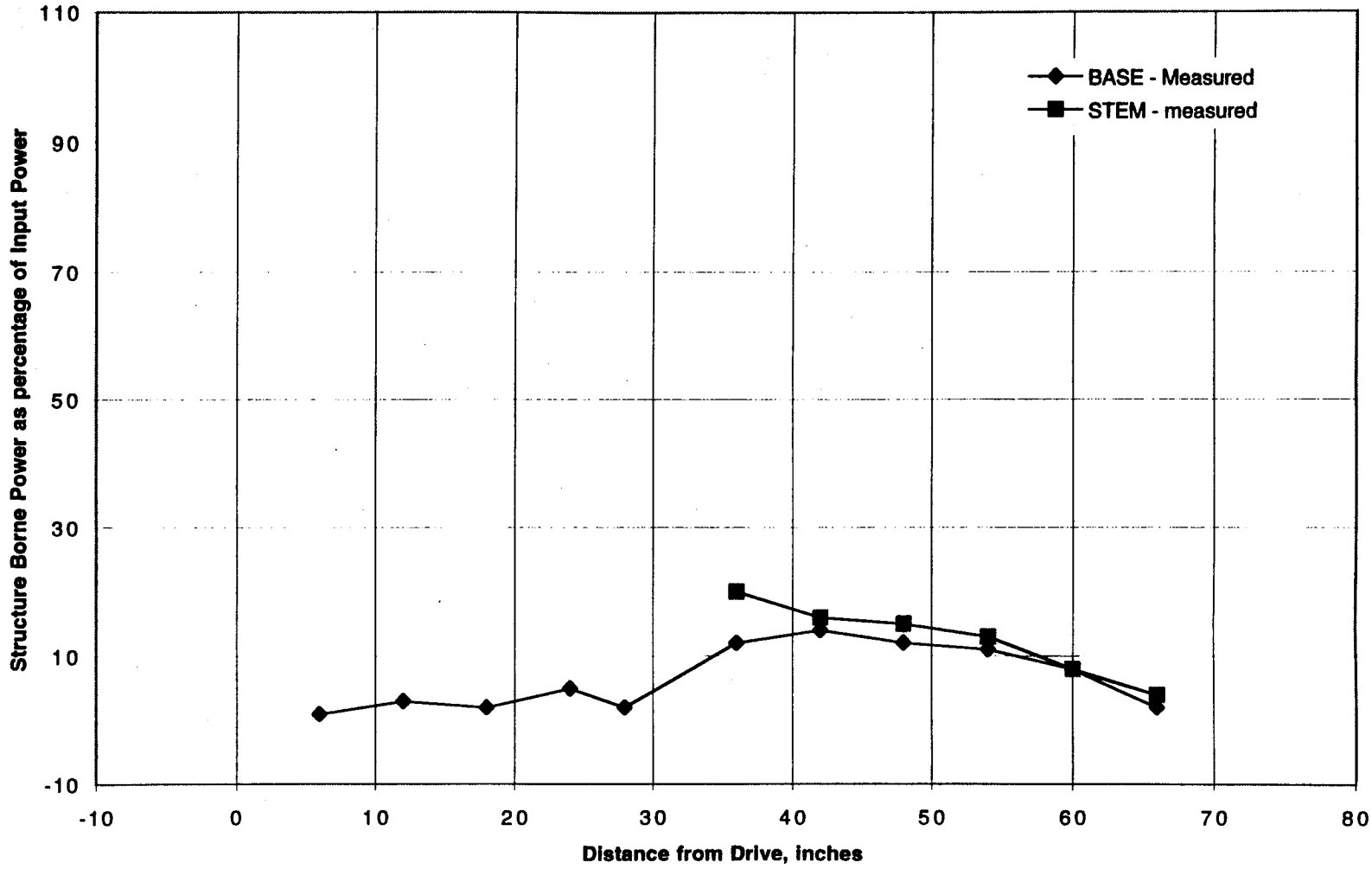

Figure 22. Flexural structure-borne powers on bolted T-beam at 735 Hz.

THIS PAGE INTENTIONALLY LEFT BLANK

Initial Distribution

Copies

1 AMRL, Defence Science and Technology Organization
- 1 C. Norwood

2 Bolt, Beranek and Newman (N.London)
- 1 R. Haberman
- 1 H. Allik

1 Brigham Young University
- 1 S. Sommerfeld

2 Cambridge Acoustical Associates
- 1 M. Junger
- 1 J. Garrelick

1 Cambridge Collaborative
- 1 G. Manning

2 CETIM
- 1 J. Tourret
- 1 G. Pavic

12 DTIC

1 Florida Atlantic University
- 1 J. Cuschieri

1 Ford Motor Company
- 1 H. Torab

4 General Dynamics (EB Div)
- 1 J. Wilder (443)
- 1 S. Gordon (443)
- 1 J. Dmitri (471)
- 1 Library

3 General Electric Corp (R&D)
- 1 H. Lee
- 1 S. Tong
- 1 D. Powell

3 Georgia Institute of Technology
- 1 K. Cunefare
- 1 J. Ginsberg
- 1 I. Berthelot

1 Iowa State University
- 1 A. Mann

2 MIT
- 1 I. Dyer
- 1 R. Lyon

14 NAVSEA
- 1 SEA 03
- 1 SEA 03H
- 1 SEA 03T
- 1 SEA 03T2
- 1 SEA 03U
- 1 SEA 03U2
- 1 SEA 03W
- 1 SEA 03X7
- 1 SEA 08
- 1 SEA 92R
- 1 PEO-SUB-R
- 1 PEO-SUB-XT
- 1 PMS 393
- 1 library

2 NKF Engineering Associates
- 1 E. Moyer
- 1 R. Miller

3 NRL
- 1 E. Williams
- 1 J. Bucaro
- 1 library

7 ONR - Ballston
- 1 R. Vogelsong
- 1 A. Tucker
- 1 Abraham
- 1 E. Rood
- 1 G. Main
- 1 J. DeCorpo
- 1 library

1 ONR - London
- 1 P. Majumdar

10 Pennsylvania State University
- 1 C. Burroughs
- 1 S. Hayak
- 1 J. Tichi
- 1 T. McDevitt
- 1 G. Koopman
- 1 M. Tretheway
- 1 D. Thompson
- 1 R. Weyer
- 1 D. Capone
- 1 R. Marboe

1 Purdue University

1 R. Bernhard

1 Technical Research Centre of Finland
1 J. Linjama

1 TNO Institute of Applied Physics
1 J. Verheij

1 University of Connecticut
1 M. Accorsi

1 Universita "La Sapienza", Rome Italy
1 A. Sestieri

2 Virginia Tech
1 C. Knight
1 R. West

2 University of Southampton
1 F. Fahy
1 Baker

NSWC/CD Distribution

1 011 Corrado
1 011 Halsall
1 011 Douglas
1 011 Kim
1 011 Caplan

1 20
1 204
1 2042 R. Cheng
1 2042 Everstine
10 2042 Hambric
1 2042 Quezon

1 3421
1 3422

1 508 Boswell
1 508 Brown
1 544 Peterson

1 60 Gaunaurd
1 65 Rockwell
1 65.1 Tinley
1 65.1 Lesar
1 69.1 Costanzo

1 70
1 7051 Blake
1 702 Maidainik
1 7052 Feit
1 72 King
1 7220 Rummerman
1 7250 Shang
1 7250 Maga
1 7250 Gershfeld
1 7250 Fisher
1 7250 Cole
1 7250 Hwang
1 7250 Carroll
10 7250 Szwerc
1 7016 Szilagyi

1 80
1 804.1 Dickey
1 84